# ARTICLES

# Proterozoic low orbital obliquity and axial-dipolar geomagnetic field from evaporite palaeolatitudes

David A. D. Evans[1]

**Palaeomagnetism of climatically sensitive sedimentary rock types, such as glacial deposits and evaporites, can test the uniformitarianism of ancient geomagnetic fields and palaeoclimate zones. Proterozoic glacial deposits laid down in near-equatorial palaeomagnetic latitudes can be explained by 'snowball Earth' episodes, high orbital obliquity or markedly non-uniformitarian geomagnetic fields. Here I present a global palaeomagnetic compilation of the Earth's entire basin-scale evaporite record. Magnetic inclinations are consistent with low orbital obliquity and a geocentric-axial-dipole magnetic field for most of the past two billion years, and the snowball Earth hypothesis accordingly remains the most viable model for low-latitude Proterozoic ice ages. Efforts to reconstruct Proterozoic supercontinents are strengthened by this demonstration of a consistently axial and dipolar geomagnetic reference frame, which itself implies stability of geodynamo processes on billion-year timescales.**

The principle of uniformitarianism, in which modern geological processes guide our conception of the ancient world, has faced a challenge in the field of Precambrian palaeoclimate. In contrast with Ordovician and younger ice ages, which are characterized by expectedly high palaeolatitudes, Proterozoic glaciogenic deposits have until now yielded purely low to moderate palaeomagnetic latitudes, including several near-equatorial results of high reliability[1,2]. A simple interpretation of these results invokes the encroachment of ice sheets across all latitudes, a model known as snowball Earth[3–5]. The concept of a 'hard' snowball with global ice cover enduring for millions of years has been controversial, with some scientists advocating partly unfrozen tropical oceans[6,7].

An alternative to global refrigeration invokes a high Precambrian planetary obliquity of more than 54°, which would reverse zonal mean-annual temperature gradients, preferentially spawning ice ages in the tropics rather than near the poles[8,9]. A single direct measure of Precambrian obliquity by using stromatolite heliotropism[10] suggests a 'normal' low value at about 630 Myr, but this isolated example should be confirmed by similar studies elsewhere. Geophysical considerations on the feasibility of the high-obliquity hypothesis are generally negative[11–13], yet the spatial distribution of Precambrian glacial deposits, which lack any well-documented high-latitude examples, currently permit both the snowball and high-obliquity models[1,2].

A non-uniformitarian Precambrian geomagnetic field may also be invoked to explain the low palaeomagnetic inclinations. Database-wide palaeomagnetic compilations indicate a shallow bias relative to random sampling of a geocentric-axial-dipole (GAD) field across the spherical surface, which may be explained by the preferential motion of continents into low latitudes, or subsidiary higher-order components to the ancient geomagnetic field[14]. Some support for the latter possibility was raised by means of numerical geodynamo modelling with spatially non-uniform core–mantle boundary conditions[15,16].

The distribution of ancient evaporite deposits can help distinguish between these non-uniformitarian alternatives. Modern tropospheric Hadley–Ferrel circulation descends on the subtropics of both hemispheres, where evaporation exceeds precipitation in today's desert belts. Fifty years ago, the emerging science of palaeomagnetism admirably succeeded in reconstructing consistent palaeoclimatic zones in the context of post-Pangaean continental drift[17–19]. Subsequent studies considered evaporitic rocks as old as the Cambrian period and found deposits concentrated in palaeolatitude bands consistent with modern evaporite belts of 15–35° latitude[20–23]. Here I revisit the evaporite palaeolatitude test according to the current palaeomagnetic data set and extend it back through Proterozoic time, to the oldest recognized examples of large evaporite basins on Earth.

## Evaporite palaeolatitudes

The world's largest Cenozoic–Mesozoic evaporite basins, with preserved salt volumes greater than $10^4$ km$^3$, are listed in Table 1; references are given in Supplementary Data. Continental reconstructions from this interval benefit from combined analysis of palaeomagnetic data from exposed rocks and seafloor anomalies (see, for example, ref. 24). The basins are distributed primarily through the 15–35° arid latitude belt as determined previously, with a $23 \pm 4°$ (95% confidence) volume-weighted mean latitude (Fig. 1) that is independent of icehouse–greenhouse global climate state and the reversal frequency of geomagnetic polarity. Consistency of this result with modern climate zones bolsters the use of ancient evaporites as palaeolatitude proxies and supports a predominantly, if not entirely, GAD geomagnetic field model for the past 230 Myr (refs 14, 25). Detailed palaeomagnetic work on Late Triassic sedimentary rocks, spanning a range of palaeoclimatic zones in the north Atlantic region, also supports a GAD geomagnetic field model[26].

Palaeozoic evaporites are widespread and voluminous, as reviewed comprehensively by Zharkov[27]. Although no seafloor-spreading data exist before the Jurassic period, Palaeozoic continental apparent polar wander (APW) paths are generally coherent enough to allow palaeolatitudes at specific ages to be calculated from running means or spline fits (see, for example, ref. 25). Palaeolatitude estimates vary

[1]Department of Geology and Geophysics, 210 Whitney Avenue, Yale University, New Haven, Connecticut 06520-8109, USA.

**Table 1 | Palaeomagnetic constraints on evaporite basin depositional latitudes**

| Evaporite basin (°N, °E) | Age (Myr) | Volume (km³) | Palaeopole (°N, °E) | Dipole $\lambda'$ (°) |
|---|---|---|---|---|
| **Cenozoic–Mesozoic (0–250 Myr)** | | | | |
| 1. Messinian (36, 018) | 5 | 1,000,000 | Present position | 36 N |
| 2. Red Sea (21, 038) | 10 | 900,000 | BC02 mean (85, 174) | 18 ± 2 N |
| 3. SW Iran (31, 047) | 20 | 300,000 | BC02 mean (84, 229) | 25 ± 3 N |
| 4. S Mozambique (−23, 035) | 20 | 27,000 | BC02 mean (84, 176) | 28 ± 3 S |
| 5. E China (34,115) | 40 | 20,000 | BC02 mean (81, 162) | 40 ± 3 N |
| 6. Rus, Arabia (25, 050) | 50 | 200,000 | BC02 mean (75, 237) | 10 ± 3 N |
| 7. N Sahara (32, 008) | 90 | 32,000 | BC02 mean (67, 249) | 19 ± 5 N |
| 8. Indochina (16, 104) | 100 | 50,000 | Y+01 mean (57, 170) | 26 ± 4 N |
| 9. S Atlantic (−3, 010) | 120 | 35,000 | BC02 mean (54, 261) | 13 ± 3 S |
| 10. Hith, Arabia (24, 050) | 150 | 360,000 | BC02 mean (47, 268) | 11 ± 6 S |
| 11. Central Asia (43, 070) | 150 | 250,000 | BC02 mean (75, 160) | 41 ± 7 N |
| 12. Andes (35, 290) | 160 | 40,000 | BC02 mean (89, 264) | 35 ± 5 S |
| 13. Gulf of Mexico (27, 265) | 160 | 2,400,000 | BC02 mean (74, 150) | 19 ± 5 N |
| 14. Alan, Arabia (33, 044) | 180 | 20,000 | BC02 mean (61, 270) | 11 ± 5 N |
| 15. Tanzania (−10, 040) | 200 | 150,000 | BC02 mean (62, 252) | 33 ± 4 S |
| 16. N Sahara (35, 355) | 200 | 710,000 | BC02 mean (62, 252) | 25 ± 4 N |
| 17. Keuper (52, 005) | 225 | 50,000 | T+01 mean (56, 132) | 26 ± 3 N |
| 18. Jilh, Arabia (29, 049) | 230 | 120,000 | TV02 mean (49, 254) | 9 ± 11 S |
| 19. S China (29, 106) | 230 | 80,000 | Z+96 mean (46, 218) | 6 ± 7 N |
| Cenozoic–Mesozoic volume-weighted mean (95% confidence) | | | | 23 ± 4 |
| **Permian–Carboniferous (250–360 Myr)** | | | | |
| 1. Zechstein (54, 011) | 250 | 200,000 | T+01 mean (52, 155) | 20 ± 2 N |
| | | | TC04,15% G3 (55, 158) | 23 |
| 2. Khuff, Arabia (27, 050) | 260 | 75,000 | TV02 mean (43, 257) | 16 ± 11 S |
| | | | TC04, interpolated (36, 243) | 26 |
| 3. E European (52, 052) | 270 | 1,100,000 | T+01 mean (45, 165) | 23 ± 3 N |
| | | | TC04,12.5% G3 (45, 167) | 22 |
| 4. Peru–Bolivia (−13, 291) | 270 | 62,000 | TV02 mean (68, 174) | 22 ± 9 S |
| | | | TC04,12.5% G3 (62, 161) | 30 |
| 5. Midcontinental USA (41, 257) | 270 | 81,000 | T+01 mean (44, 126) | 6 ± 3 N |
| | | | TC04, 12.5% G3 (44, 128) | 7 |
| 6. Amazon (−3, 310) | 300 | 25,000 | TV02 mean (60, 174) | 24 ± 6 S |
| | | | TC04, 10% G3 (55, 158) | 33 |
| 7. Sverdrup (79, 264) | 315 | 120,000 | V93 mean (28, 129) | 20 ± 4 N |
| | | | TC04, 10% G3 (36, 127) | 28 |
| 8. Canadian Maritime (46, 298) | 340 | 46,000 | TC04 mean (19, 118) | 25 S |
| | | | TV02, 20% G3 (7, 136) | 34 |
| Permian–Carboniferous volume-weighted mean (95% confidence) | | | | 21 ± 4 |
| Recalculated for G3 contributions (95%) | | | | 23 ± 4 |
| **Devonian–late Ediacaran (360–600 Myr)** | | | | |
| 1. E European (57, 040) | 370 | 1,100,000 | V93 mean (27, 149) | 13 ± 8 N |
| 2. Taimyr (74, 115) | 370 | 18,000 | TC04 mean (10, 117) | 26 N |
| 3. W Canada (55, 250) | 390 | 86,000 | V93 mean (23, 110) | 5 ± 8 S |
| 4. Morsovo (53, 033) | 400 | 81,000 | CT02 mean (2, 145) | 11 S |
| 5. Michigan (41, 279) | 420 | 29,000 | CT02 mean (14, 125) | 30 S |
| 6. Canning (−21, 124) | 440 | 26,000 | CT02 mean (19, 201) | 5 N |
| 7. Canadian Arctic (76, 265) | 460 | 19,000 | CT02 mean (13, 149) | 7 N |
| 8. Mackenzie (65, 234) | 500 | 110,000 | CT02 mean (4, 165) | 12 N |
| 9. Morocco–Iberia (34, 357) | 520 | 50,000 | Debated | —— |
| 10. Siberia (60, 105) | 520 | 800,000 | Tommotian–Toyonian | (8–25) S |
| 11. Persian Gulf (22, 058) | 545 | 500,000 | Sinyai (−33, 326)* | 13 ± 4 N |
| 12. Salt Range (33, 073) | ~550 | 240,000 | Khewra (−28, 032) | 18 ± 11 S |
| Devonian–Ediacaran volume-weighted mean (95% confidence) | | | | 14 ± 2 |
| **Precambrian (pre-Ediacaran; >600 Myr)** | | | | |
| 1a. Skillogalee (−31, 138) | ~770 | 25,000 | Mundine Well (46, 135)* | 13 ± 4 |
| 1b. Curdimurka (−30, 138) | ~785 | 50,000 | None | – |
| 2a. Kilian–Redstone River (68, 238) | ~770 | 30,000 | Direct (22, 151) | 21 ± 9 |
| 2b. Minto Inlet (68, 238) | ~800 | 90,000 | L. Dal Basinal (−16, 141) | 17 ± 3 |
| 3. Duruchaus (−22, 018) | ~800 | 15,000 | None | – |
| 4. Copperbelt (−12, 027) | ~830? | 25,000 | None | – |
| 5. Centralian (−25, 129) | ~830 | 140,000 | Browne (−44, 312) | 20 ± 5 |
| 6. Borden (73, 278) | ~1,200 | 15,000 | Strathcona S. (8, 204) | 12 ± 3 |
| 7. Char/Douik (23, 352) | ~1,200? | 8,000 | None | – |
| 8. Belt (48, 245) | 1,460 | 10,000 | Belt B1-4 (−25, 214)* | 12 ± 2 |
| 9. Discovery (−25, 118) | ~1,500 | ≤2,800 | None | – |
| 10a. Balbirini (−17, 136) | 1,610 | 2,500 | Direct (−66, 178) | 34 ± 6 |
| 10b. Lynott (−17, 136) | 1,635 | 3,000 | Direct (−75, 163) | 30 ± 6 |
| 10c. Myrtle (−19, 138) | 1,645 | 13,000 | Emmerugga (−79, 203) | 23 ± 6 |
| 10d. Mallapunyah (−19, 138) | 1,660 | 5,000 | Direct (−35, 214) | 22 ± 3 |
| 10e. Corella (−21, 140) | 1,740 | 2,000 | Peters Creek (−26, 221)* | 17 ± 5 |
| 11. Stark (62, 248) | ~1,870 | 30,000 | Stark (−15, 212) | 8 ± 8 |
| 12. Rocknest (67, 246) | ~1,950 | 1,000 | Western R. (14, 341) | 11 ± 9 |
| 13. Juderina (−26, 120) | ~2,100 | 1,000 | None | – |
| 14. Tulomozero (63, 35) | ~2,100 | 1,000 | Kuetsyarvi (25, 301)* | 20 ± 13 |
| 15. Chocolay (47, 275) | ~2,250 | 4,500 | Lorrain (−46, 268) | 3 ± 3 (?) |
| Pre-Ediacaran volume-weighted mean (95% confidence) | | | | 17 ± 3 |

Evaporite localities represent the centres of the basins. Dipole $\lambda'$ is the palaeolatitude of the basin centre assuming a GAD magnetic field; 95% uncertainties are from ($A_{95}$) or (dp) confidence limits on the palaeomagnetic poles. Poles are rotated into the coordinate reference frame of the evaporite basin, with Euler parameters from the cited sources, plus the Sinyai pole to Arabia from ref. 29. In some instances, vertical-axis rotations of the palaeomagnetic sample localities are known or suspected, but they are not corrected here. Abbreviations: G3, same-sign geocentric axial octupole component; BC02, ref. 24; CT02, ref. 47 (no uncertainties on means provided); T+01, ref. 48; TC04, ref. 39 (no uncertainties provided); TV02, ref. 25; V93, ref. 28; Y+01, ref. 49; Z+96, ref. 50. For further information and references on evaporite deposits and palaeomagnetic poles, see Supplementary Information.
* Individual palaeomagnetic studies derived wholly or partly from volcanic rocks.
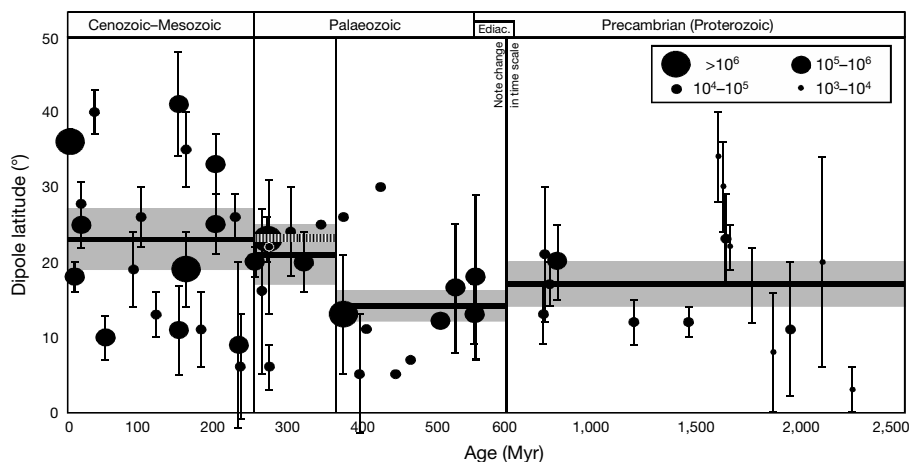
**Figure 1 | Evaporite palaeomagnetic latitudes through time, assuming a GAD field as a null hypothesis.** Individual basins are schematically scaled to evaporite volume (circle sizes are scaled in km$^3$ as in the inset) and shown with 95% uncertainty limits in palaeolatitude as listed in Table 1. Volume-weighted means (solid bars) and 95% error envelopes (shaded) are divided into the four age intervals as discussed in text. A corrected mean for best-fit octupole components can be calculated for the late Palaeozoic (dashed bar; uncertainty excluded for clarity).

little with averaging method or data selection, except for the age intervals of the Silurian–Devonian and the Early Cambrian[28,29], at times of widespread evaporite deposition (Table 1). For basins of these ages, special care was taken to consult primary constituent palaeomagnetic studies in order to determine which latitude estimates are most reliable. In the present compilation, the Palaeozoic (and late Ediacaran) basins are separated into two groups: Permian–Carboniferous, for which quantitative estimates of octupolar field components are available through palaeogeographic consistency tests across large continents[25,30], and Devonian–Ediacaran, for which no such estimates currently exist. Eight Permian–Carboniferous deposits with volumes greater than 10$^4$ km$^3$ have a weighted-mean dipole palaeolatitude of 21 ± 4°, nearly identical to the Cenozoic–Mesozoic mean and nearly unaffected when previously estimated octupolar components are included in the pole calculations (Table 1). Among 11 out of 12 large Devonian–Ediacaran evaporites with palaeomagnetic constraints, however, the weighted-mean dipole palaeolatitude of 14 ± 2° is substantially lower (Fig. 1) and is again independent of global climate state and geomagnetic reversal frequency. As discussed below, this result is anomalous and may indicate exceptional periods of non-uniformitarian geomagnetism and/or palaeoclimate.

An extensive literature survey of described Precambrian evaporite deposits highlights 21 examples of great thickness and basin-wide scale (Table 1), the largest of which have also appeared in previous compilations[31,32]. Continuous APW paths are rarely determined for segments of Precambrian time, so the estimation of palaeolatitudes requires specific results from the evaporite units themselves, conformably bounded strata, or coeval rocks on the same palaeocontinent. Evaporites with volumes greater than 10$^3$ km$^3$ are restricted to the Proterozoic era, as old as about 2,250 Myr. The volume-weighted mean inclination from the 15 palaeomagnetically constrained basins among this group (31.6 ± 2.1° (s.e.m.)) corresponds to a GAD palaeolatitude of 17 ± 3° (95% confidence). This result is slightly lower than the Cenozoic–Mesozoic baseline value, with possible causes discussed below.

### Testing high obliquity

Three published general-circulation climate models have reported evaporation–precipitation trends as a function of latitude on a high-obliquity planet with otherwise Earth-like parameters[33–35]. These simulations indicate a near-isothermal to weakly reversed mean-annual zonal climate pattern, depending on whether the oceans are allowed to store and release heat through the annual cycle. Whenever there is any annually averaged evaporative peak present, the models locate this maximum at a single arid belt centred on the Equator. In conjunction with an assumed GAD field, these simulations would predict a unimodal peak of evaporite palaeomagnetic latitudes at 0°, with a large standard deviation.

Precambrian evaporite latitudes on Earth show a significantly non-zero mean with low variance (Table 1), consistent with a 'normal' climate gradient on a low-obliquity world. A zero mean could be obtained if half of the palaeolatitudes were considered to represent the opposite hemisphere (geomagnetic polarity being generally unknown in the Precambrian), but even then the total distribution would be significantly bimodal, in contrast with the high-obliquity model predictions. For some basins the palaeomagnetic record is complete enough to show continental motion through alternate times of evaporite and carbonate deposition, in patterns consistent with latitude crossings between subtropical arid and equatorial humid zones (Fig. 2). The Precambrian volume-weighted mean evaporite basin latitude (17 ± 3°) is indistinguishable from that of the entire Phanerozoic eon (20 ± 3°). Given that Phanerozoic obliquity is universally considered to have modern-like values[9], the palaeomagnetic record of evaporites thus argues for uniformitarian orbital dynamics of the Earth–Moon system at least as old as the Palaeoproterozoic era.

### Testing non-dipole field components

The second application of evaporite palaeolatitudes considers the long-term structure of the geomagnetic field. Although one can conceive of an infinitely complex hypothetical Precambrian geomagnetic field topology, only axial components can be distinguished through broad palaeoclimatic comparisons spanning billions of years. Because palaeomagnetic polarity is generally unknown among sparse Precambrian results, tests for subsidiary geomagnetic field components are practically limited to antisymmetric harmonics such as the geocentric axial octupole. Figure 3 shows the effect on surface inclinations of 0–40% subsidiary zonal octupole of the same sign relative to an otherwise pure GAD field[36], for the 15° and 35° latitudinal bounds of the modern arid zones and for the mean depositional latitudes of Cenozoic–Mesozoic evaporite basins. Only the Devonian–Ediacaran subset shows a significantly shallower mean inclination at the 99% confidence level (Student's $t$-test), which could be interpreted as a persistent octupolar component of 19% relative to the dipole. This value is broadly similar in magnitude to that of the aggregate database-wide inclination tests of Kent and Smethurst[14], who found a best-fit same-sign octupole component of about 25% for pre-Mesozoic data. Using the Cenozoic–Mesozoic evaporite inclination baseline, an octupolar contribution of this magnitude shifts the expected inclination range to 21.9 ± 2.5° (s.e.m.). Although pre-Ediacaran data are slightly shallower than the Cenozoic–Mesozoic GAD baseline, they are significantly different at the 99% confidence level (Student's $t$-test) from that 25% octupole-adjusted baseline value. This suggests that substantial non-GAD components were not present in the long-term Precambrian geomagnetic field, and it supports the alternative explanation for database-wide inclination shallowing proposed by Kent and Smethurst[14],
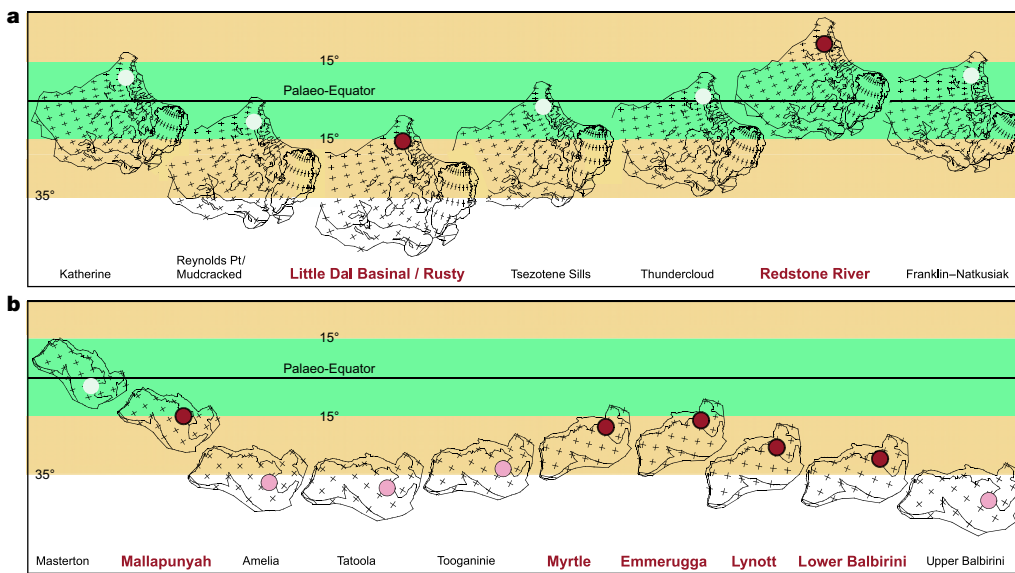
**Figure 2 | Two sporadically evaporitic pre-Ediacaran basins that are palaeomagnetically well constrained throughout their depositional histories.** The horizontal axis denotes stratigraphic development, with younger to the right. Latitude zones are colour-coded for the present-day humid tropics and arid subtropics, on a Mercator projection. Darker, lighter, and white circles indicate stratigraphic intervals of major, minor, and absent-to-negligible evaporites, respectively. **a**, Neoproterozoic Amundsen basin, Laurentia[45]. **b**, Palaeoproterozoic McArthur basin, northern Australia[46].

namely that continental positions tend on average towards low latitudes by means of true polar wander through supercontinental cycles[37]. Such a tendency would similarly impart a low-latitude bias to the preserved subset of rift-related evaporites, but the largest basins considered here are found in variable tectonic settings that should be independent of supercontinental episodicity.

A significant octupole component (about 10–15% relative to GAD) was determined by consistency tests on palaeomagnetic data from the late Palaeozoic continents Laurussia[30] and Gondwanaland[25], and this also resolved some long-standing overlap problems with reconstructions of Pangaea between those two plates (a pure GAD model requires a large Permian megashear between the two continents[38]). The present compilation of evaporite inclinations does not provide further insight into this debate, because error-min-

imizing octupole field corrections for Permian to Late Carboniferous APW paths[39] have no significant effects on the volume-weighted mean for evaporites of that interval (Table 1). Octupole-corrected early Palaeozoic APW paths are not yet available for all continents, but such calculations will help to determine whether the early part of the Palaeozoic era was a time of departure from an otherwise uniformitarian GAD field, perhaps as a result of particular convective patterns at the core–mantle boundary[15].

Other factors may have contributed to the substantially shallowed mean inclination for Devonian–Ediacaran evaporites, and the slightly shallowed mean for pre-Ediacaran evaporites: first, narrowing of the Hadley zones due to a faster rotation rate[40]; second, a shallow bias of palaeomagnetic inclinations due to sedimentary magnetization processes[41]; and third, particular continental distributions conducive to aridity in deep tropical regions[23,42]. The first process may have contributed to the shallowing of Precambrian inclinations but not substantially to the more marked early Palaeozoic anomaly. Regarding the second process, the pre-Ediacaran mean remains low even when only igneous-based palaeomagnetic results are considered (Table 1). The significantly shallowed early Palaeozoic mean evaporite palaeolatitude could be a result of the third process, because several of the larger basins reconstruct near the vertex of a proto-Tethys-like sea[39], which may have been influenced by monsoon-like circulation in the same manner that produces anomalously dry conditions in present-day eastern Africa[23]. The slightly shallowed pre-Ediacaran mean inclination could also reflect one or more instances of similar palaeoclimatic peculiarities.

## Implications

First-order consistency of Precambrian evaporite basin palaeomagnetic latitudes with modern arid zones and Cenozoic–Mesozoic evaporite palaeolatitudes confirms the GAD hypothesis for the Earth's magnetic field since about 2,000 Myr ago, about four times longer than known from previous palaeoclimatic–palaeomagnetic global comparisons[2,21,22]. Because no voluminous evaporites are preserved from the times of Proterozoic ice ages, the present study allows the possibility of relatively short-term geomagnetic departures from the GAD model, as a potential contributor to the low glacial palaeolatitudes. However, those departures would need to be extreme to produce the near-equatorial results, and, on the contrary, stratabound antiparallel palaeomagnetic polarity reversals from within some of the Proterozoic glaciogenic successions[43] seem to reflect 'typical' geomagnetic behaviour of more recent times. Short-term departures from low Earth obliquity are not possible because of the stabilizing influence of the Moon[11].
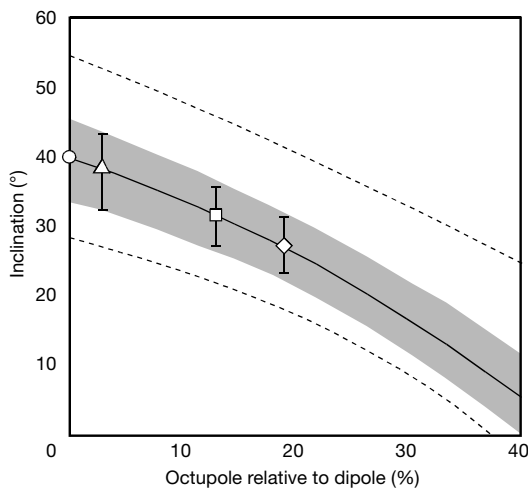


**Figure 3 | Plot of magnetic inclination against same-sign geomagnetic octupole component relative to a purely GAD field.** The values for the inclination biases were calculated from the equation in ref. 36. Dashed curves indicate the declining inclination values, according to increasing octupole contributions, that would correspond to 15° and 35° latitude limits of present arid subtropical zones. The solid curve corresponds to the same biasing effect on inclinations computed from the mean latitude of Cenozoic–Mesozoic evaporite basins and a pure GAD field (circle), with its 95% error envelope (shaded). Permian–Carboniferous (triangle), Devonian–Ediacaran (diamond), and pre-Ediacaran (square) mean inclinations and their 95% uncertainty limits, when aligned with the Cenozoic–Mesozoic baseline curve, provide quantifiable estimates of ancient geomagnetic octupole field components.

Earth's evaporite record extends in abundance only through the Proterozoic Eon[31,32]; studies such as this are therefore unlikely to characterize the growth of Earth's geomagnetic field, which seems to have occurred before 2,450 Myr ago[44]. Conversely, reliable palaeomagnetic data from Archaean sedimentary rocks are currently so sparse as to preclude comprehensive treatment of any palaeoclimatic indicator from that interval, evaporitic or otherwise. Nonetheless, the present compilation addresses several important issues of deep time: first, that the high-obliquity hypothesis has failed an important observational test that is independent of Earth's Precambrian glacial record; second, that near-equatorial palaeomagnetic latitudes of Precambrian glacial deposits are not likely to be substantially biased by non-dipolar field components, unless such components were of exceptional magnitude and short duration coincident with ice ages; and third, that—according to the available tests—Earth's time-averaged magnetic field may be approximated by a geocentric axial dipole for most of the past 2 Gyr. Success of the uniformitarian principle in explaining evaporite distributions implies that its failure, with regard to low-latitude Precambrian glaciation, is most probably caused by anomalies in palaeoclimatic rather than geophysical processes.

1. Evans, D. A. D. Stratigraphic, geochronological, and paleomagnetic constraints upon the Neoproterozoic climatic paradox. *Am. J. Sci.* **300**, 347–433 (2000).
2. Evans, D. A. D. A fundamental Precambrian–Phanerozoic shift in Earth's glacial style? *Tectonophysics* **375**, 353–385 (2003).
3. Hoffman, P. F., Kaufman, A. J., Halverson, G. P. & Schrag, D. P. A Neoproterozoic snowball Earth. *Science* **281**, 1342–1346 (1998).
4. Hoffman, P. F. & Schrag, D. P. The snowball Earth hypothesis: Testing the limits of global change. *Terra Nova* **14**, 129–155 (2002).
5. Kirschvink, J. L. in *The Proterozoic Biosphere: A Multidisciplinary Study* (eds Schopf, J. W. & Klein, C.) 51–52 (Cambridge Univ. Press, Cambridge, 1992).
6. Hyde, W. T., Crowley, T. J., Baum, S. K. & Peltier, W. R. Neoproterozoic 'snowball Earth' simulations with a coupled climate/ice sheet model. *Nature* **405**, 425–429 (2000).
7. Poulsen, C. J. Absence of a runaway ice-albedo feedback in the Neoproterozoic. *Geology* **31**, 473–476 (2003).
8. Williams, G. E. Late Precambrian glacial climate and the Earth's obliquity. *Geol. Mag.* **112**, 441–465 (1975).
9. Williams, G. E. History of the Earth's obliquity. *Earth Sci. Rev.* **34**, 1–45 (1993).
10. Vanyo, J. P. & Awramik, S. M. Stromatolites and Earth–Sun–Moon dynamics. *Precambr. Res.* **29**, 121–142 (1985).
11. Levrard, B. & Laskar, J. Climate friction and the Earth's obliquity. *Geophys. J. Int.* **154**, 970–990 (2003).
12. Pais, M. A., Le Mouel, J. L., Lambeck, K. & Poirer, J. P. Late Precambrian paradoxical glaciation and obliquity of the Earth: A discussion of dynamical constraints. *Earth Planet. Sci. Lett.* **174**, 155–171 (1999).
13. Williams, D. M., Kasting, J. F. & Frakes, L. A. Low-latitude glaciation and rapid changes in the Earth's obliquity explained by obliquity-oblateness feedback. *Nature* **396**, 453–455 (1998).
14. Kent, D. V. & Smethurst, M. A. Shallow bias of paleomagnetic inclinations in the Paleozoic and Precambrian. *Earth Planet. Sci. Lett.* **160**, 391–402 (1998).
15. Bloxham, J. Sensitivity of the geomagnetic axial dipole to thermal core–mantle interactions. *Nature* **405**, 63–65 (2000).
16. Olson, P. & Christensen, U. R. The time-averaged magnetic field in numerical dynamos with non-uniform boundary heat flow. *Geophys. J. Int.* **151**, 809–823 (2002).
17. Irving, E. Palaeomagnetic and paleoclimatological aspects of polar wandering. *Geofis. Pura Appl.* **33**, 23–41 (1956).
18. Irving, E. & Briden, J. C. Palaeolatitude of evaporite deposits. *Nature* **196**, 425–428 (1962).
19. Opdyke, N. D. in *Continental Drift* (ed. Runcorn, S. K.) 41–65 (Academic, New York, 1962).
20. Borchert, H. & Muir, R. O. *Salt Deposits* (Van Nostrand, London, 1964).
21. Drewry, G. E., Ramsay, A. T. S. & Smith, A. G. Climatically controlled sediments, the geomagnetic field, and trade wind belts in Phanerozoic time. *J. Geol.* **82**, 531–553 (1974).
22. Gordon, W. A. Distribution by latitude of Phanerozoic evaporite deposits. *J. Geol.* **83**, 671–684 (1975).
23. Parrish, J. T., Ziegler, A. M. & Scotese, C. R. Rainfall patterns and the distribution of coals and evaporites in the Mesozoic and Cenozoic. *Palaeogeogr. Palaeoclimatol. Palaeoecol.* **40**, 67–101 (1982).
24. Besse, J. & Courtillot, V. Apparent and true polar wander and the geometry of the geomagnetic field over the last 200 Myr. *J. Geophys. Res.* **107**, doi:10.1029/2000JB000050 (2002).
25. Torsvik, T. H. & Van der Voo, R. Refining Gondwana and Pangea palaeogeography: estimates of Phanerozoic non-dipole (octupole) fields. *Geophys. J. Int.* **151**, 771–794 (2002).
26. Kent, D. V. & Tauxe, L. Corrected Late Triassic latitudes for continents adjacent to the North Atlantic. *Science* **307**, 240–244 (2005).
27. Zharkov, M. A. *History of Paleozoic Salt Accumulation* (Springer, Berlin, 1981).
28. Van der Voo, R. *Paleomagnetism of the Atlantic, Tethys and Iapetus Oceans* (Cambridge Univ. Press, Cambridge, 1993).
29. McElhinny, M. W., Powell, C. M. & Pisarevsky, S. A. Paleozoic terranes of eastern Australia and the drift history of Gondwana. *Tectonophysics* **362**, 41–65 (2003).
30. Van der Voo, R. & Torsvik, T. H. Evidence for late Paleozoic and Mesozoic non-dipole fields provides an explanation for the Pangea reconstruction problems. *Earth Planet. Sci. Lett.* **187**, 71–81 (2001).
31. Pope, M. C. & Grotzinger, J. P. Paleoproterozoic Stark Formation, Athapuscow basin, northwest Canada: Record of cratonic-scale salinity crisis. *J. Sedim. Res.* **73**, 280–295 (2003).
32. Warren, J. K. *Evaporites: Their Evolution and Economics* (Blackwell Science, Oxford, 1999).
33. Hunt, B. G. The impact of large variations of the Earth's obliquity on the climate. *J. Meteorol. Soc. Jpn* **60**, 309–318 (1982).
34. Jenkins, G. S. Global climate model high-obliquity solutions to the ancient climate puzzles of the Faint Young Sun Paradox and low-altitude Proterozoic Glaciation. *J. Geophys. Res.* **105**, 7357–7370 (2000).
35. Jenkins, G. S. High-obliquity simulations for the Archean Earth: Implications for climatic conditions on early Mars. *J. Geophys. Res.* **106**, 32903–32913 (2001).
36. Livermore, R. A., Vine, F. J. & Smith, A. G. Plate motions and the geomagnetic field. I. Quaternary and late Tertiary. *Geophys. J. R. Astron. Soc.* **73**, 153–171 (1983).
37. Evans, D. A. D. True polar wander and supercontinents. *Tectonophysics* **362**, 303–320 (2003).
38. Muttoni, G. *et al.* Early Permian Pangea 'B' to Late Permian Pangea 'A'. *Earth Planet. Sci. Lett.* **215**, 379–394 (2003).
39. Torsvik, T. H. & Cocks, L. R. M. Earth geography from 400 to 250 Ma: a palaeomagnetic, faunal and facies review. *J. Geol. Soc. Lond.* **161**, 555–572 (2004).
40. Hunt, B. G. The effects of past variations of the Earth's rotation rate on climate. *Nature* **281**, 188–191 (1979).
41. Tauxe, L. Inclination flattening and the geocentric axial dipole hypothesis. *Earth Planet. Sci. Lett.* **233**, 247–261 (2005).
42. Hallam, A. Continental humid and arid zones during the Jurassic and Cretaceous. *Palaeogeogr. Palaeoclimatol. Palaeoecol.* **47**, 195–223 (1984).
43. Raub, T. D. & Evans, D. A. D. Magnetic reversals in basal Ediacaran cap carbonates: A critical review. *Eos* **87** (36), abstract GP41B–02 (2006).
44. Smirnov, A. V., Tarduno, J. A. & Pisakin, B. N. Paleointensity of the early geodynamo (2.45 Ga) as recorded in Karelia: A single-crystal approach. *Geology* **31**, 415–418 (2003).
45. Park, J. K. & Jefferson, C. W. Magnetic and tectonic history of the Late Proterozoic Upper Little Dal and Coates Lake Groups of northwestern Canada. *Precambr. Res.* **52**, 1–35 (1991).
46. Idnurm, M. Towards a high resolution Late Palaeoproterozoic – earliest Mesoproterozoic apparent polar wander path for northern Australia. *Aust. J. Earth Sci.* **47**, 405–429 (2000).
47. Cocks, L. R. M. & Torsvik, T. H. Earth geography from 500 to 400 million years ago: a faunal and paleomagnetic review. *J. Geol. Soc. Lond.* **159**, 631–644 (2002).
48. Torsvik, T. H., Van der Voo, R., Meert, J. G., Mosar, J. & Walderhaug, H. J. Reconstructions of the continents around the North Atlantic at about the 60th parallel. *Earth Planet. Sci. Lett.* **187**, 55–69 (2001).
49. Yang, Z., Yin, J., Sun, Z., Otofuji, Y. & Sato, K. Discrepant Cretaceous paleomagnetic poles between Eastern China and Indochina: a consequence of the extrusion of Indochina. *Tectonophysics* **334**, 101–113 (2001).
50. Zhao, X., Coe, R. S., Gilder, S. A. & Frost, G. M. Palaeomagnetic constraints on the palaeogeography of China: implications for Gondwanaland. *Aust. J. Earth Sci.* **43**, 643–672 (1996).

nine of the ten species studied[3], there are data on worker reproduction in queenless colonies where there can be no policing in favour of the queen's eggs. Two things change as a result. First, freed from policing, a higher fraction of workers opt to lay eggs. But, remarkably, many individuals still help instead of reproducing, and the fraction that help is now positively correlated with relatedness. Relatedness does matter, and this must be the reason that coercion can induce workers to help.

Wenseleers and Ratnieks[5] earlier found a similar result when nutritional coercion is absent. In honeybees and their relatives the stingless bees, most species use nutritional coercion to limit queen production to a few at a time. Few are needed, because new queens can reproduce only by usurping the mother queen, or by acquiring a colony on the rare occasions the colony splits into two. The exception is the stingless bee genus *Melipona*. Here, all brood cells are pre-provisioned equally, and then sealed. A developing larva can therefore choose for herself whether to develop as a queen, with a larger abdomen, or as a worker, with larger fore parts (Fig. 1). Many females choose to develop as queens, showing their preference in the absence of constraint. This can result in hundreds of surplus young queens in a colony, so a new level of control has evolved. The workers slaughter the excess queens, so that the

nest evokes the climactic scene of Hamlet, with royal corpses littering the stage. This is a great waste, but shows that it is nutritional coercion that normally keeps queen numbers in check. Yet this case, too, reveals that coercion is not everything and relatedness is important. More than 75% of females still choose the altruistic worker role, and the proportion is higher in species with higher relatedness[5].

Finally, it should be remembered that Hamilton's kinship theory is not just about altruism *per se*, but about how all traits of altruistic workers evolve. When honeybee ancestors first evolved sociality, the workers could not waggle dance to convey information to each other, or suicidally detach their stings to better repel enemies, or police each other. These features, and all specialized features of workers, had to evolve by kin selection, through their indirect effects on relatives who could pass on genes for these traits. For example, the surprising positive correlation between relatedness and worker laying[3], which has been confirmed in a much larger comparative study[4], is expected under policing. Low relatedness among workers favours workers policing each other. Thus, although policing keeps suppressed workers from fully expressing their kin-related interests, policing is itself kin selected.

Many social conflicts create winners and losers. But only kinship allows evolution to make

creative use of the social losers, turning them into reproductive police, exquisite communicators and heroic defenders. When Hamlet suffered the slings and arrows of outrageous fortune, he debated putting an end to himself. Social insect workers do sometimes choose suicide but, because of kinship, this hamiltonian choice is profoundly different from the hamletian dilemma. The stinging honeybee worker commits suicide when her sting is torn out, but this saves her kin. She is not making an escape from outrageous fortune, but making the best of it — not fearful of what dreams may come, but hopeful for what genes may come. However socially constrained her life may have been, her last action makes her own clear statement: long live the kin! ■

David C. Queller is in the Department of Ecology and Evolutionary Biology, Rice University, PO Box 1892, Houston, Texas 77251-1892, USA.
e-mail: queller@rice.edu

1. Hamilton, W. D. *J. Theor. Biol.* **7,** 1–52 (1964).
2. Field, J., Cronin, A. & Bridge, C. *Nature* **441,** 214–217 (2006).
3. Wenseleers, T. & Ratnieks, F. L. W. *Nature* **444,** 50 (2006).
4. Wenseleers, T. & Ratnieks, F. L. W. *Am. Nat.* www.journals. uchicago.edu/cgi-bin/resolve?id=doi:10.1086/508619
5. Wenseleers, T. & Ratnieks, F. L. W. *Proc. R. Soc. Lond. B* **271,** S310–S312 (2004).
6. West-Eberhard, M. J. *Q. Rev. Biol.* **50,** 1–33 (1975).
7. Queller, D. C. & Strassmann, J. E. *BioScience* **48,** 165–175 (1998).
8. Ratnieks, F. L. W. *Am. Nat.* **132,** 217–236 (1988).

## GEOPHYSICS

# Same old magnetism

Edward Irving

**Latitudes at which ancient salt deposits occur show that Earth's magnetic field has always aligned along its rotation axis. One possible implication is that ancient global glaciations were not caused by a realignment of this axis.**

In a paper of admirable scope and thoroughness that appears on page 51 of this issue[1], David Evans analyses the magnetization locked into rocks associated with salts from all over the globe that have been deposited over the past 2,500 million years. Taking as a working model the 'geocentric axial dipole' — the idea that, averaged over thousands of years, the magnetic field at Earth's surface resembles the field of a magnet, or dipole, at Earth's centre[2,3] — these magnetizations and this model provide clues to the past evolution and interplay of Earth's magnetism, climate and geography.

In the geocentric axial dipole model, the north and south poles of Earth's internal magnet are aligned along Earth's axis of rotation. This simple axial form is thought to be caused by rotational forces that guide the motions of Earth's conducting liquid core, and so constrain the average surface field. Under favourable circumstances, rocks become magnetized along the direction of the ambient geomagnetic

field as they are formed. Thus, by sampling sequences of rocks with formation dates spanning several thousands of years, one can determine the past average direction of the field, the 'palaeolatitude' of the sampling locality and the position of the palaeomagnetic pole at the time. For the past 5 million years, these poles coincide with the present rotational pole; the giant dipole model has therefore been valid for at least this long.

For rocks of much earlier ages, the palaeomagnetic poles determined from rocks from different sampling sites are widely dispersed. This is the result of continental drift and seafloor spreading in the intervening period. If we restore the continents to their original positions using the geometrical methods of plate tectonics, palaeomagnetic pole positions agree very well[4]. Such corrections go back some 200 million years, and again imply that the geomagnetic field has been a geocentric dipole for that period.

But this evidence does not tell us that the field was also axial. To determine this, one first assumes that the geocentric axial dipole model holds, and determines the latitudes at which temperature-sensitive deposits were laid down from their magnetization directions, or, in the case of salts, those of similarly aged rocks. If these palaeolatitudes are compatible with the modern latitudes of similar deposits, the geocentric axial dipole model is likely to be valid.

The deposits that are the object of Evans's studies[1] are known as evaporites. They comprise beds of, among other things, gypsum, anhydrite, halite and potassium salts, and are of huge economic importance. They were formed by intense evaporation of enclosed saline lakes or sea water. The conditions for their formation must therefore have been hot and dry, as expected typically in latitudes lower than 30°. Very near the Equator, however, it is too wet for them to form.

Evans shows that, consistently over the past 2,500 million years, evaporites have been deposited predominantly between latitudes 10° and 35° (Fig. 1, overleaf). This is a beautifully documented testament to uniformitarianism — the doctrine that today's geological processes have always occurred in a broadly similar manner.

Interest in the interplay between the geomagnetic field and ancient climate zones has been spurred by evidence in a wide range of latitudes, including at sea level near the Equator,

## NATURE

### 50 YEARS AGO

Not being English or French, but of speech a mid-west American from Manitoba and Dakota, it did not mean anything to me when in 1906 I heard the Eskimos of the Mackenzie Delta and north-eastern Alaska speaking of spruce gum as 'kutsuk'... Years later, perhaps in 1912, I learned that the word for the gum of a Brazilian plant, and of other South American plants, is 'caoutchouc'... Turning now to Greenland, in Sam. Kleinschmidt: "Den Grönlandske Ordbog", I find "kutsuk... Gummi, Campher og lignende producter"... When I first began to talk about this, I was told it was coincidence. But the intellectual climate is changing, among other things in linguistics, and now... [some] think 'connexion' a likelier word than 'coincidence'. **Vilhjalmur Stefansson**
From *Nature* 3 November 1956.

### 100 YEARS AGO

*Great Bowlers and Fielders. Their Methods at a Glance* by G. W. Beldam and C. B. Fry — Following up their interesting volume on "Great Batsmen," the accomplished authors of "Great Bowlers and Fielders" have practically completed all that action photography can teach us regarding the methods of the great cricketers. The present

handsome volume with its 464 action photographs registers for all time the successive positions of the body in the act of bowling of some of the most celebrated bowlers of our day, and also certain very characteristic attitudes of a number of our best fielders... [This] one represents W. Rhodes at the beginning of his final swing, and is chosen partly because of the perfection with which the grip of the ball is indicated.
From *Nature* 1 November 1906.

## 50 & 100 YEARS AGO



**Figure 1 | Ancient evaporite.** This white-coloured sulphate evaporite cliff (about 10 metres high) is interbedded with grey carbonate and mudstone layers within the 800-million-year-old Minto Inlet Formation on Victoria Island in northern Canada. Palaeomagnetic results from age-equivalent rocks in northwestern Canada indicate a latitude of 17° at the time of deposition that is consistent with modern arid climate zones.

that intermittent periods of glaciation covered the whole Earth between 750 million and 550 million years ago. Theories abound as to why this should have occurred, and one proposal[5] is that Earth's obliquity might have changed drastically at the time. Obliquity is the tilt of Earth's equatorial plane to its ecliptic — the plane of its orbit around the Sun — and is currently 23.5°. If this tilt exceeds around 58°, high latitudes would get more solar heat than low latitudes, and this could account for low-latitude glaciations. The new data[1] prove problematic for such models. Before and after the global glaciations, Evans consistently finds a strong low-latitude, off-Equator peak in evaporite deposition, indicating that obliquity then was not very different from now.

Evans's calculated palaeolatitudes do vary slightly through time, which he divides into four intervals running backwards. These are: interval 1, 250 million years ago (Myr) to the present; interval 2 (370–250 Myr); interval 3 (600–370 Myr); and interval 4 (2,500–600 Myr). The evaporite latitudes do tend to be lower in intervals 4, 3 and 2 than in interval 1, but the changes are irregular. There are two chief explanations for this variation. The first is that before interval 1 the geomagnetic field had long-term axial non-dipole components that endured unchanged for millions of years. These could have perturbed the geomagnetic field sufficiently to cause palaeomagnetic estimates of latitudes based on the geocentric axial

dipole model to be systematically too low by as much as 10°. Alternatively, the field could have remained a simple axial dipole throughout, with the aberrations reflecting, for instance, continental drift or polar wandering.

Evans provides strong evidence for the validity of the geocentric axial dipole model throughout interval 1. Before that, he notes arguments[6] favouring long-term axial non-dipole fields in interval 2, finds no grounds for them in interval 4, and seems undecided about interval 3.

I will focus on interval 2. Here, Evans accepts the previously advanced view[6] that Alfred Wegener's grouping of continents into a super-continent[7], known as Pangaea A, persisted, not greatly changed, back through the entire interval. There are significant problems with such a long-lived Pangaea. Although there are firm correlations[8] throughout interval 2 of very thick stratigraphic sequences within Gondwana and within Laurussia (respectively the clustered southern and northern continents that came together to form Pangaea A), there are no comparable correlations between Gondwana and Laurussia. Thus, placing these two supercontinents together in Pangaea A during interval 2 is problematic. Palaeomagnetic data[9] for late interval 2 based on the assumption of an axial geocentric dipole field place portions of northern Gondwana at the same latitude as southern Laurussia, implying an impossible overlap of the two continents, one on top of the other, of around 1,000 km. But invoking the long-term axial non-dipole components would not remove this overlap[9], because in such low latitudes their effect would be small and equal in both places. It is worth noting, too, that Evans's analysis does not explicitly require long-term axial non-dipole components in interval 2.

Evans makes no steady overall commitment to either of the contending explanations for the variations in the evaporite palaeolatitudes. I hope I will be forgiven for doing so. It seems reasonable to me to take the estimates of evaporite latitudes at face value and accept that, during the past 2,500 million years — apart from a relatively brief global glaciation at the end of interval 4 — hot and dry climates were typical of tropical, but not equatorial, latitudes, and that long-term non-dipole components have always been small or negligible. In other words, one should accept the geocentric axial dipole model as demonstrably successful for interval 1 and use it to settle questions of palaeogeography in earlier intervals. For example, displacing Gondwana to the east during interval 2 by around 3,500 km, a palaeogeography known as Pangaea B, reconciles the palaeomagnetic data with a feasible configuration of the early continents[9].

Such palaeogeographic solutions are more generally testable than solutions involving long-term non-dipole fields: whereas the geomagnetic dynamo in early ages is an awfully remote item, ancient strata can be directly studied and the phenomena they reflect described. Most

researchers accept interval 2 palaeogeography as settled. I disagree: on the principle of working from the known to the unknown, it could be just the issue that needs further critical consideration before we can confidently approach the question of earlier climate zones. Data of the extensive nature supplied by Evans[1] are what is needed to inform such debates. ■

Edward Irving is an emeritus scientist at the Pacific Geoscience Centre, Geological Survey of Canada, Department of Natural Resources, PO Box 6000, Sidney, British Columbia V8L 4B2, Canada.
e-mail: tirving@pgc-gsc.nrcan.gc.ca

1. Evans, D. A. D. Nature 444, 51–55 (2006).
2. Gilbert, W. (transl. Mottelay, P. F.) De Magnete (1600) (Dover, Mineola, NY, 1958).
3. Hospers, J. J. Geol. 63, 59–74 (1955).
4. Besse, J. & Courtillot, V. J. Geophys. Res 107, doi:10.1029/200JB000050 (2002).
5. Williams, G. E. Earth Sci. Rev. 34, 1–45 (1993).
6. Torsvik, T. H. & Van der Voo, R. Geophys. J. Int. 151, 771–794 (2002).
7. Wegener, A. (transl. Skerl, J. G. A.) Origin of Continents and Oceans (Methuen, London, 1924).
8. Du Toit, A. L. Our Wandering Continents (Oliver & Boyd, Edinburgh, 1937).
9. Muttoni, G. et al. Earth. Planet. Sci. Lett. 215, 379–394 (2003).

## CANCER BIOLOGY

# Second step to retinal tumours

Valerie A. Wallace

**The mutations that cause retinoblastoma are well known, but how they enable the cancer to evade controls on cell division was unclear. Secondary mutations affecting a growth-regulatory pathway have now been identified.**

Most cancers arise through a two-step process in which an initiating mutation requires further tumour-promoting mutations to instigate the full-blown disease. Retinoblastoma is a childhood cancer of the retina that is one of the few tumour types for which the initiating genetic lesion is known — both copies of the retinoblastoma (Rb) tumour-suppressor gene are inactivated. However, few of the additional tumour-promoting lesions have been identified. On page 61 of this issue, Laurie et al.[1] report that amplification of the numbers of MDMX and MDM2 genes occurs frequently in human retinoblastoma. They show that increased expression of MDMX can promote tumour development in genetic models of retinoblastoma in mice. They also show that a drug called nutlin-3, which blocks some actions of MDM proteins, can stop tumour progression in the eye, opening up a promising avenue for the potential treatment of these tumours.

MDMX and MDM2 are structurally related proteins that act as antagonists of a cell-signalling pathway named after its most famous member — the tumour suppressor p53 (ref. 2). The p53 protein is a gene regulatory factor that normally inhibits cell proliferation and induces cell death in response to cellular stress. The Rb tumour-suppressor pathway also inhibits cell proliferation, in part by blocking the expression of genes required for the cell to divide. Normally, loss of Rb leads to induction of p14$^{ARF}$, a key activator of p53 (ref. 3; Fig. 1). But in many cancers, p53 activity is blocked by mutations in the p53 gene or alterations to other genes in the pathway, allowing cells to escape death and leading to uncontrolled division. In human retinoblastoma, however, the p53 pathway is intact[4], and acute Rb loss in

the human retina induces p14$^{ARF}$ expression, which should unleash the lethal potential of p53 in response to this mutation[1]. So how do retinoblastoma cells subvert the intact p53 pathway to prevent it from killing them?

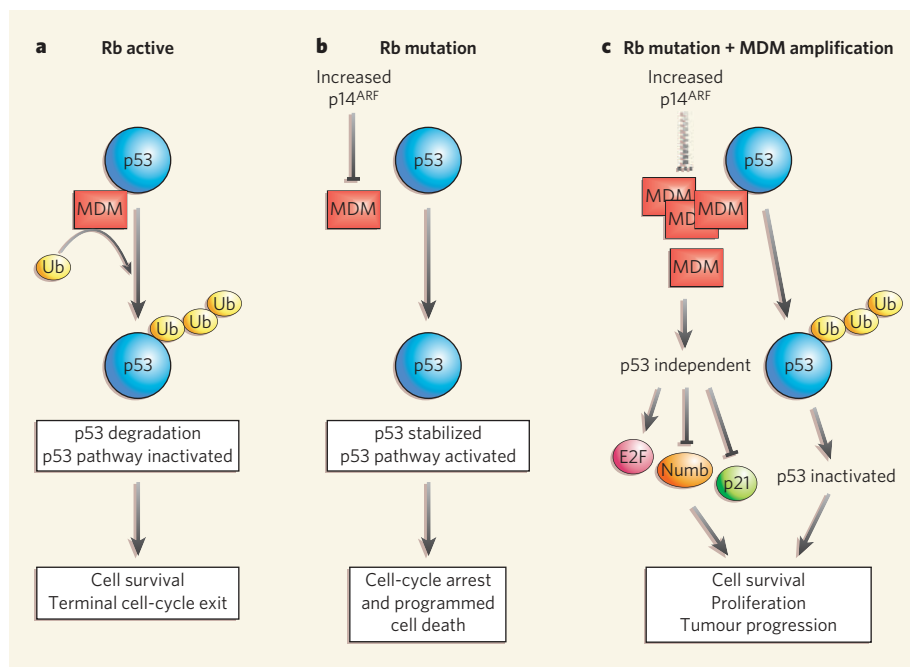Laurie et al. provide evidence that the p53 pathway is circumvented in retinoblastoma cells

by increased expression of MDMX or MDM2. These proteins interact with p53, blocking its gene-regulatory activity and promoting its degradation[2] (Fig. 1). Analysis of human retinoblastoma reveals that the number of MDMX and MDM2 genes is amplified in 65% and 10% of the tumours, respectively, and that this correlates negatively with p53 levels. Moreover, the levels of MDMX RNA and protein were increased in several recently removed human tumours, and the authors confirm that MDMX antagonizes p53-mediated activation of certain target genes, cell-cycle arrest and programmed cell death in retinoblastoma cell lines.

To investigate the functional significance of the MDMX protein in the development of retinoblastoma, the authors turned to mouse models and cultured human fetal retina tissue (retinal explants). In the mouse, the development of retinoblastoma requires the elimination of Rb and one additional Rb family member, either p130 or p107 (ref. 5). However, as occurs in humans, the tumours in these models can develop with intact p53. Laurie et al. show that MDMX expression inhibits cell death, promotes proliferation and exacerbates retinoblastoma progression in mice lacking Rb and p107. MDMX expression also blocks cell death and promotes proliferation in human fetal retinal explants where Rb expression was reduced experimentally. This effect was not observed with an MDMX mutant that does not bind to p53. Furthermore, in both the mouse and the human retinal models, MDMX



**Figure 1 | Role of MDM proteins in retinoblastoma. a,** Under normal conditions, levels of p53 protein are kept low, partly through negative regulation by MDM proteins. MDM2 is an enzyme that tags p53 with a ubiquitin molecule (Ub), thereby promoting p53 degradation. MDMX also interacts physically with p53 and inhibits its gene-regulatory activity. **b,** Mutation of the retinoblastoma gene (Rb) results in increased production of the p14$^{ARF}$ protein, which in turn leads to inactivation of MDM2, thus promoting p53 pathway activation. This leads to cell-cycle arrest or cell death, or facilitates DNA repair. **c,** Increased expression of MDM proteins in the absence of Rb blocks activation of p53, leading to survival of the abnormal cells and tumour progression. Independently of p53, interactions of MDM with other proteins that regulate cell division, survival and differentiation could also promote tumour progression[13].

SUPPLEMENTARY INFORMATION

The most substantial Phanerozoic evaporite basins, by total volume of halite plus sulphate salts, are selected mainly from the compendia in refs.[1-6]. Because Phanerozoic evaporites are extensively described, more detailed reference lists are not provided here. In each instance, a palaeomagnetic latitude is calculated for a reference locality from the center of the existing or inferred area of the original depositional basin, and an age near the middle of the span of evaporite deposition. Except for some terranes within the Tethyan foldbelt of Asia (e.g., Khorat basin, Indochina), Late Triassic and younger basins can be reconstructed to palaeolatitudes by combining continental and oceanic palaeomagnetic data via the global plate circuit[7]. An independent compilation of data[8] produces practically identical results. Mid-Triassic to Late Cambrian palaeolatitudes are calculated from running means along apparent polar wander (APW) paths from global palaeomagnetic syntheses, most notably refs. [9-11]. Two of these studies[9, 10] do not include error estimates in their tabulated mean pole positions, but they are likely to be in the range of ca.10° (ref. [12]).

Estimated Cambrian and late Ediacaran evaporite palaeolatitudes require explanation because during this interval of time, continental motions and most APW paths appear to show rapid motion[13-16], and accurate age constraints plus tectonic affinities are of exceptional importance in calculating basin palaeolatitudes. Pre-Ediacaran evaporites are also discussed individually, as numbered in Table 1. In many instances, thicknesses and basin areas must be estimated from illustrations in the cited references. Most Precambrian evaporites are not composed of original salts, but are indicated by secondary

pseudomorph replacements after the original chlorides or sulphates[5, 17]. I have considered

bedded magnesite in my compilation[18], but not more tentative suggestions of evaporites

based on substantially different inferrred ocean chemistry (e.g. Hamersley-type iron

formations[19]). Depositional palaeolatitudes noted below are valid for a geocentric-axial-

dipolar (GAD) field on a sphere of constant radius.

(9) Morocco-Iberia. Alvaro et al.[20] summarize evaporitic pseudomorphs averaging an

estimated 200 m in thickness across an area of ca.1250 x 200 km within the Cadomian

belt and the Moroccan Cambrian platform. Ages range from the oldest strata,

Adoudounian, containing an ash bed dated by U-Pb on zircon at 525.38±0.46 Ma

[21], to the overlying Lie de Vin succession, dated at 522±2 Ma[22], to European strata

correlative with the Moroccan Issafen unit, dated at 517±1.5 Ma[22]. The most abundant

halite pseudomorphs are found in Iberian strata of approximately 520 Ma age, according

to the regional correlations[20]. At about that time, the Cadomian belt was adjacent to the

West African sector of Gondwanaland, drifting rapidly together toward the south pole,

according to both palaeoclimate indicators[20] and a smoothed Gondwanaland APW path[23].

The precise timing of the palaeomagnetic rotations, however, are uncertain[16, 24, 25], thus

Table 1 lists these Early Cambrian evaporites' palaeolatitudes as "debated."

(10) Siberia. Zharkov[6] assigned area and volume estimates of the extensive Cambrian

halite and gypsum beds of the southwestern Siberian craton. Petrychenko et al.[26] indicate

salt depositional ages spanning the Tommotian to Toyonian intervals of the Early

Cambrian (ca.520 Ma; ref. [22]). Similar to the case of Gondwanaland, Early Cambrian

palaeomagnetic poles for Siberia are also debated.  A more conservative interpretation of data[27, 28] indicates minor APW for that interval, but "anomalous" older results[29] have been reproduced by some studies (e.g., ref. [30]).  The range of Tommotian-Toyonian evaporite palaeolatitudes indicated by these studies is 08-25°; its midpoint of 17° is used in the mean calculations.

(11-12) Persian Gulf-Salt Range.  A widespread evaporitic basin, developed during latest Precambrian time on the proto-Tethyan margin of Gondwanaland, is now exposed in fragments between Arabia and western India[31].  The Arabian strata, with numerous minor evaporite levels culminating upward toward the halite-bearing Ara Formation at the top of the Huqf Supergroup[32] are precisely dated at 545-542 Ma[33, 34].   In northern Pakistan, the gypsum-bearing Salt Range Formation occupies a similar stratigraphic position beneath a sparsely fossiliferous Cambrian succession[35].  The Hanseran evaporites of western India may correlate with those deposits[36], but precise age constraints are lacking. Palaeomagnetic data bearing on depositional palaeolatitudes must be applied indirectly from other regions of Gondwanaland (in the case of the precisely dated Ara Formation) or from stratigraphically adjacent strata (in the case of the Salt Range Formation).  After restoration of Neogene separation between Arabia and Africa (all Gondwanaland reconstruction parameters from ref. [25]), a palaeomagnetic pole from the 547±4 Ma Sinyai metadolerite[37] implies a palaeolatitude of 15° for the Ara Formation in Oman.  Another estimate of ca.15° Ara palaeolatitude is provided by the coeval upper Arumbera Sandstone in Australia[38], assuming that Gondwanaland had formed by earliest Cambrian time[39].  For the Salt Range and Hanseran evaporites, with less precisely constrained ages,

depositional palaeolatitudes of ca.17° are provided by the conformably overlying Khewra

Formation in the Salt Range[40].  Although all these palaeolatitudes are similar, the pole

positions are quite distinct and suggest either diachroneity among evaporite deposits or

final tectonic assembly of Gondwanaland after their deposition.

(1) Skillogalee-Curdimurka, South Australia.  Within the Adelaide foldbelt, two

prominent levels of evaporites are described.  The older, Curdimurka Subgroup of the

Callanna Group, contains abundant pseudomorphs after anhydrite, halite, and shortite,

attaining an aggregate thickness of about 1 km over an area of about 50,000 km$^2$ (refs. [41, 42]).  The evaporitic sequence lies above the Rook Tuff dated at 802±10 Ma[43] and is

considered to be older than the 777±7 Ma Boucaut Volcanics (C.M.Fanning,

unpublished, quoted in ref. [44]).  No reliable palaeomagnetic data exist from this age

interval in Australia.  The younger level of evaporites is found as bedded magnesite in the

upper Skillogalee Formation, within the Burra Group, averaging about 500 m thickness

across the same rift structures that localized deposition in the underlying Curdimurka

Subgroup[18, 41, 44].  The dated Boucaut Volcanics are considered to correlate with the

lowermost Burra Group, providing a maximum age constraint on the Skillogalee

magnesites.  For a minimum age constraint, the overlying Sturtian glacial deposits are

correlated globally to the broad interval of 740–720 Ma[45] or perhaps as young as ca.710

Ma[46].  Within this interval, the 755±3 Ma Mundine Well Dykes of Western Australia

provide a reliable palaeomagnetic pole[47] that implies a palaeolatitude of 13° for the Burra

Group, assuming a GAD field and tectonically coherent Australia in the mid-Neoproterozoic[48].

(2) Kilian-Minto Inlet, Amundsen Basin, Canada. Two thick evaporite levels have been correlated among Precambrian inliers of the Amundsen basin in northern Canada[49]. In the Mackenzie Mountains, the lower level is located immediately and conformably above strata that are intruded by 780-Ma sills of the Gunbarrel large igneous province[50], whereas the upper level lies disconformably above basalts that are traditionally correlated with those sills[51]. The lower level comprises the Minto Inlet Formation on Victoria Island, plus the correlative Gypsum Formation in the Mackenzie Mountains, and attains a typical thickness of 300 m across an interpolated depositional basin area of ca.300,000 $km^2$ (refs. [49, 52, 53]). The upper level is represented by basal portions of the Kilian Formation on Victoria Island and the Redstone River Formation in the Mackenzie Mountains, totalling about 100 m thickness across the same area[49, 54]. Various palaeomagnetic studies of these successions have shown migration of the Laurentian continent back and forth through the tropics during the broad time spanning the two evaporite-rich intervals[55, 56]. In elegant confirmation of uniformitarian palaeoclimate zonation, the evaporites were deposited during the two migrations of the Amundsen basin through subtropical palaeolatitudes (using poles from the Little Dal "basinal" member for the Minto Inlet/Gypsum evaporite, and directly from the Redstone River Formation for the upper evaporite); whereas carbonate deposition predominated during times of near-equatorial palaeolatitude.

(3) Duruchaus, Namibia.  A ca.500 m thick and moderately extensive (about 30,000 km$^2$) evaporite succession, the Duruchaus Formation, is preserved at the northwestern margin of the Kalahari craton in the southern external zone of the Damara orogen[57].  Age constraints on the Duruchaus evaporites are poor, relying on overlying, Sturtian-equivalent glacial deposits for an approximate 740–720 Ma minimum age[45, 58], and no well defined maximum age other than presumption of deposition generally during the rift stage of the Damara orogenic cycle (ca.800 Ma[59]).  Because of these poor age constraints, and more importantly, a dearth of palaeomagnetic data for this general time interval from the Kalahari craton, there is no estimable depositional palaeolatitude for the Duruchaus evaporites.

(4) Copperbelt, central Africa.  The central-African Copperbelt contains basin-scale evaporites that are largely inferred from enormous solution-induced "gigabreccias" [60].  The Roan Supergroup, which contains the evidence for evaporites, is bracketed in age by the nonconformably underlying 883±10 Ma Nchanga Granite[61] and the overlying 765±5 Ma basal volcanics of the Kundelungu Group[62].  Inferred total thickness of the Roan evaporites is approximately 500 m, spread across a basin area of ca.50,000 km$^2$ (ref. [60]).  New correlations of Roan strata with a metasedimentary succession in the Zambezi belt[63], the latter being intruded by the ca.820-Ma Lusaka Granite (S. Johnson and B. de Waele, pers. comm.), suggest a tentative pre-820 Ma age for the Roan evaporites.  If so, then no palaeomagnetic data from the Congo-São Francisco craton are available to estimate evaporitic palaeolatitudes of the copperbelt.

(5) Centralian superbasin, Australia. The most extensive pre-Ediacaran evaporite deposit, covering an aggregate area of ca.140,000 km$^2$ across most of central Australia, with a typical thickness of ca.800 m of bedded gypsum, anhydrite, and halite, is represented by the Gillen Member of the Bitter Springs Formation (Amadeus region), plus correlatives such as the Browne Formation (Officer region) and upper Sunbeam Group (Savory region)[64-67]. None of the regions are constrained tightly in age, but they are well correlated to each other. In addition, integrated stratigraphic and micropalaeontological comparisons with the Adelaide foldbelt[66] suggest that the evaporites correlate to strata underlying the 802-Ma Rook Tuff[43]. Direct palaeomagnetic study of the Browne Formation on azimuthally unoriented drillcore suggested a depositional palaeolatitude of 11° or 13°, depending on whether the data were treated with single or dual magnetic polarity[68]. Subsequent palaeomagnetic work on oriented borehole material indicates a higher palaeolatitude of 20° (ref. [69]), both for the borehole locality and for a reference locality toward the center of the Centralian superbasin (Table 1).

(6) Borden basin, Canada. Gypsum pseudomorphs are distributed throughout ca.100 m of thickness within the lower Society Cliffs Formation on northern Baffin Island, and correlative strata in northwestern Greenland[70, 71]. Higher in the sedimentary succession, the Elwin Subgroup contains rare halite pseudomorphs[70]. The basin spans ca.140,000 km$^2$, and the total volume of evaporites is estimated at ca.15,000 km$^3$. Palaeomagnetic data from several levels of the Borden basin strata[72] indicate modest plate motion of the Laurentian craton following deposition of the basal Nauyat volcanics (considered to

correlate with the Mackenzie large igneous province at 1270 Ma[73]). The palaeomagnetic pole for the Strathcona Sound Formation, lying between the evaporitic Society Cliffs and Elwin Formations, indicates a depositional palaeolatitude of 12° (ref. [72]). This pole position lies between those from the 1235 Ma Sudbury dykes and the 1163 Ma lower Gardar volcanics[74], suggesting an age of ca.1200 Ma for the Borden evaporites that is in agreement with Pb/Pb ages on interstratified carbonates[71].

(7) Char/Douik Group, West Africa. In the Taoudeni cratonic cover succession of Mauritania, the basal Char Group contains minor halite pseudomorphs[75, 76], as does the correlative Douik Group in Algeria[76]. The thickness of evaporitic horizons is not great (ca.50 m), but the basinal area is large (ca.800 x 200 km). Although the age of the Char Group is commonly quoted as ~1000 Ma, this is based on imprecise Rb-Sr determinations[77] that are considered here as unreliable. More recent studies suggest an older, Mesoproterozoic age (e.g., ref. [78]). The Char Group has yielded various palaeomagnetic remanence directions, with a high-unblocking-temperature component interpreted as primary[79]. Evans[45], however, noted the antipolarity of this component relative to a Permian-Carboniferous overprint commonly observed across West Africa[80]. If reliable, this component would imply a palaeolatitude of 12° for the Char Group, but in the present analysis it is omitted.

(8) Belt basin, North America. Two broad levels of pseudomorphs after evaporites, or their metamorphic products, are documented[81]. The lower level is found within the

Waterton, Altyn, and Prichard Formations and their correlative units near the base of the Belt Supergroup, and is evidenced by numerous features such as pseudomorphs after gypsum and anhydrite, length-slow chalcedony, and chicken-wire textures, distributed sporadically through several hectometers of strata[82, 83]. The upper evaporitic level, within the Wallace Formation in the carbonate-rich middle part of the Belt Supergroup, is better documented. Hietanen[84] extensively described stratiform scapolite distributed in many thin layers throughout ca.400-500 m of strata within central Idaho. From the lower-grade eastern exposures of the basin, Grotzinger[85] described halite pseudomorphs within the 1-10 m-thick sedimentary cycles in the middle of the formation. Together, these studies suggest about 100 m total stratigraphic thickness, across an exposed area of about 300 km x 200 km. Restoration of Laramide shortening in the region would suggest an original outcrop area of ca.100,000 km$^2$. The lower evaporitic horizons are intruded by mafic sills dated at 1468-1469 Ma[86, 87], whereas the upper horizons conformably underlie a felsic ash bed dated at 1454±9 Ma[88]. Palaeomagnetic data are consistent throughout the lower Belt succession[89], and a grand mean including data from sedimentary and igneous rocks, yields a palaeolatitude of 12±2° for initial Belt deposition.

(9) Discovery Formation, Bangemall basin, Western Australia. Although several stratigraphic levels within the Bangemall basin are noted as evaporitic, the thickest and most widespread is within the Discovery Formation, a silicified deep-water shale containing rhombic pseudomorphs interpreted as replacing original sulphates[90]. The unit averages 70 m in thickness over a preserved area of about 40,000 km$^2$. The corresponding volume estimate is viewed as a maximum for evaporitic contribution, and

even then this unit barely passes the cutoff for consideration in this paper. As summarised by Martin and Thorne[91], the age constraints on the Edmund Group, which is the lower portion of the Bangemall Supergroup and which contains most of the evaporitic horizons, lie between about 1620 and 1465 Ma. No reliable palaeomagnetic data exist from the west Australian craton to constrain Edmund Group depositional palaeolatitudes in this imprecise age interval[48].

(10) McArthur-Mt Isa basins, northern Australia. An evaporitic contribution to the sediments deposited between ca.1750 and 1600 Ma, exposed across northern Australia, has been discussed and debated for nearly 30 years[5, 92-94]. The main evidence for evaporitic contributions to the sediments are pseudomorphs after gypsum and halite, and cauliflower chert. Five distinct ages of relatively voluminous evaporitic conditions can be distinguished. The oldest level, comprising scapolite, albite, and tourmaline associations in the Corella Formation of the eastern Isan foldbelt (pages 209-212 of ref. [5]), is estimated to total ca.500 m thickness across a narrow outcrop belt of 200 x 20 km. Depositional ages of 1750-1725 Ma are determined from U-Pb dating of interbedded volcanic ashes, as summarised by Betts et al.[5]. The interval 1790-1725 Ma shows only minor palaeomagnetic apparent polar wander for the north Australian craton[48], therefore high-quality palaeomagnetic data from the 1725-Ma Peters Creek Volcanics[95] are chosen to provide a representative palaeolatitude of 17° for the Corella meta-evaporites.

The second voluminous evaporitic horizon in the McArthur-Mt Isa basin is associated with the Mallapunyah, Paradise Creek, and Esperanza Formations[92, 93, 96]. With an

estimated age of ca.1660 Ma[97], the Mallapunyah Formation is directly studied

palaeomagnetically, providing a pre-fold remanence with stratabound polarity reversals[98].

This indicates a depositional palaeolatitude of 22° for a reference locality in the center of

the McArthur-Mt Isa basin (Table 1). Meta-evaporites of the Staveley Formation in the

eastern Isan foldbelt (p.212-213 of ref. [5]) correlate broadly to this stratigraphic level[99].

The third, most voluminous, evaporite succession in the basin corresponds with the

Myrtle and Emmerugga Formations in the Batten trough toward the west[92, 100], Karns

Dolomite on the Wearyan shelf[101], Walford Dolomite on the southern flank of the

Murphy inlier[102], Shady Bore Quartzite on the Lawn Hill platform[103], and Kennedy

Siltstone in the Mt Isa region toward the east[104]. These levels may not correlate precisely,

but numerous U-Pb ages show them to be contemporaneous within five million years at

ca.1645 Ma[97]. At the temporal resolution of this study, they can be grouped into a single

evaporitic interval, of ca.200 m thickness averaged across the entire McArthur-Mt Isa

region, with a central depositional palaeolatitude of 23° determined through direct

palaeomagnetic studies of the Myrtle and Emmerugga Formations[95, 98]. Although those

two studies yielded nearly identical results, the Emmerugga pole is used here because a

positive fold test makes it demonstrably more reliable.

The fourth evaporitic level in the McArthur-Mt Isa basin is localised within the Batten

trough, comprising the Hot Spring and Donnegan Members in the middle and upper parts

of the Lynott Formation[92] dated at 1636±4 Ma[97]. This unit is the thickest evaporite in the

McArthur basin, with cauliflower cherts, crystal gypsum pseudomorphs, and halite casts

distributed widely through a stratigraphic interval of ca.300 m. The Lynott Formation has yielded a palaeomagnetic pole, which although lacking field stability tests, lies reasonably between more reliable results of slightly older and younger ages[95]. It is tentatively used here to provide a depositional palaeolatitude of 30° for the Lynott Formation, with little influence on the pre-Ediacaran mean due to its small volume.

The final McArthur basin evaporite is evidenced by halite casts, sulphate pseudomorphs and nodules, cauliflower chert, and rare possible shortite, within a 250-m interval of the lower Balbirini Formation[105], dated at 1609-1613 Ma[97]. As with the older Lynott evaporite level, the lower Balbirini evaporitic unit is restricted to the ca.100 x 100 km Batten trough. Palaeomagnetic results from the Balbirini Formation show a pre-folding remanence[98] that is distinguishable between lower and upper units across a cryptic paraconformity[95]. These results indicate a 34° depositional palaeolatitude for the lower Balbirini evaporites.

(11) Stark Formation, Slave craton, Canada. The most voluminous Palaeoproterozoic evaporite basin is located across a large region of the Slave craton in northwestern Canada. Although identify evaporitic influence upon a wide stratigraphic range within the Great Slave Lake Supergroup[106-108], the largest evaporite is associated with the Stark Formation, in the form of megabreccia and abundant pseudomorphs after halite and gypsum[17]. The Stark Formation is intruded by the 1865±15 Ma Compton Laccoliths[109], and regional tectonic correlations with the Wopmay orogen farther north suggest an age younger than ca.1880 Ma, and a total evaporitic basin area of ca.300,000 $km^2$ (refs. [17, 110]).

Reconstructed thickness of the Stark evaporites is on the order of 100 m (ref. [17]). Direct palaeomagnetic constraints place the Stark Formation at 8° palaeolatitude[111]. This result, rotated locally about a vertical axis[112] with no effects on palaeolatitude, is bolstered by stratabound polarity reversals as well as the same direction demonstrated to be pre-folding in the immediately overlying Tochatwi Formation[113].

(12) Rocknest shelf, Slave craton, Canada. Grotzinger[114] describes halite casts and rare gypsum/anhydrite pseuodomorphs distributed throughout roughly half of the thickness of a tufa shoal facies in the Rocknest passive margin of the western Slave craton. This facies spans an area of about 250 x 50 km, and further evaporitic sedimentation is contained within an interior lagoon about 200 km wide. From these data, I estimate a total evaporitic volume on the order of $10^3$ km$^3$. The Rocknest carbonates are dated between 1963±6 Ma and 1882±4 Ma, according to volcanic ash horizons below and above the platform[115]. Using palaeomagnetic data from the "Western River" (now renamed Rifle) Formation[116], a palaeolatitude of 11° is suggested for the Rocknest platform with its minor evaporitic component.

(13) Juderina Formation, Yilgarn craton, Western Australia. Abundant pseudomorphs after gypsum and anhydrite are described from the ca.100 m-thick Bubble Well Member of the Juderina Formation, across a ca.100 x 100 km area along the northern margin of the Yilgarn craton[117]. Carbon-isotopic data from this unit are highly enriched in $^{13}$C; this observation plus loose numerical age constraints suggest an age of about 2100 Ma for the

Bubble Well evaporites (see below). No palaeomagnetic data are available from rocks of this age on the Yilgarn craton, thus depositional palaeolatitudes are unconstrained.

(14) Tulomozero Formation, Karelian craton, Russia. Melezhik et al.[118, 119] describe numerous relict evaporitic textures throughout ca.500 m of the Tulomozero Formation dolomite within the Lake Onega region of the southern Karelian craton. These carbonates contain the worldwide positive "Lomagundi" carbon-isotope excursion[120] that, if representing a singular event, is dated between 2220 and 2060 Ma[121]. The same isotopic excursion is recorded in carbonates of the northern Baltic shield, which are conformably overlain by lavas of the Kuetsyarvi Volcanic Formation. Palaeomagnetism of this latter volcanic unit[122] indicates a palaeolatitude of 20±13° for the Lake Onega region, assuming the Karelian craton was intact by ca.2100 Ma.

(15) Chocolay-Gordon Lake succession, Superior craton, Canada-USA. Larue[123] described pseudomorphs after gypsum and anhydrite from a ca.100 m-thick portion of the Chocolay Group of the Lake Superior region, distributed over a ca.400 x 100 km region in northern Michigan and Minnesota. This succession has been correlated with the upper part (Cobalt Group) of the Huronian Supergroup of southern Ontario (reviewed in ref. [124]), where a 40 m-thick basal portion of the Gordon Lake Formation contains anhydrite nodules and breccia bodies, associated with redbeds, that are attributed to a sabkha depositional environment[125, 126]. The Gordon Lake strata are intruded by the ca.2220-Ma Nipissing diabase[127, 128] and are probably substantially younger than the 2450-Ma Copper Cliff Rhyolite[129] at the base of the 10-km thick Huronian succession. Farther to the

northeast along the southern Superior craton margin, tourmalinites within the Mistassini Formation[130] could correlate with the other evaporitic units. The best estimate of a depositional palaeolatitude for these strata derives from the Lorrain Formation, conformably underlying the Gordon Lake unit. A palaeomagnetic depositional latitude of 3° is indicated[131], although Hilburn et al.[132] question the reliability of that result and suggest that Cobalt Group palaeolatitudes remain unconstrained.

**Supplementary References**

1. Alsharhan, A. S. & Nairn, A. E. M. Sedimentary Basins and Petroleum Geology of the Middle East (Elsevier, Amsterdam, 1997).

2. Hallam, A. Continental humid and arid zones during the Jurassic and Cretaceous. Palaeogeography, Palaeoclimatology, Palaeoecology 47, 195-223 (1984).

3. Hardie, L. A. The roles of rifting and hydrothermal $CaCl_2$ brines in the origin of potash evaporites: An hypothesis. American Journal of Science 290, 43-106 (1990).

4. Parrish, J. T., Ziegler, A. M. & Scotese, C. R. Rainfall patterns and the distribution of coals and evaporites in the Mesozoic and Cenozoic. Palaeogeography, Palaeoclimatology, Palaeoecology 40, 67-101 (1982).

5. Warren, J. K. Evaporites: Their Evolution and Economics (Blackwell Science, Oxford, 1999).

6. Zharkov, M. A. History of Paleozoic Salt Accumulation (Springer-Verlag, Berlin, 1981).

7. Besse, J. & Courtillot, V. Apparent and true polar wander and the geometry of the geomagnetic field over the last 200 Myr. Journal of Geophysical Research 107 (2002).

8. Schettino, A. & Scotese, C. R. Apparent polar wander paths for the major continents (200 Ma to the present day): a palaeomagnetic reference frame for global plate tectonic reconstructions. Geophysical Journal International 163, 727-759 (2005).

9. Cocks, L. R. M. & Torsvik, T. H. Earth geography from 500 to 400 million years ago: a faunal and paleomagnetic review. Journal of the Geological Society, London 159, 631-644 (2002).

10. Torsvik, T. H. & Cocks, L. R. M. Earth geography from 400 to 250 Ma: a palaeomagnetic, faunal and facies review. Journal of the Geological Society, London 161, 555-572 (2004).

11.    Torsvik, T. H. & Van der Voo, R. Refining Gondwana and Pangea palaeogeography: estimates of Phanerozoic non-dipole (octupole) fields. Geophysical Journal International 151, 771-794 (2002).

12.    Van der Voo, R. Paleomagnetism of the Atlantic, Tethys and Iapetus Oceans (Cambridge University Press, Cambridge, 1993).

13.    Evans, D. A. True polar wander, a supercontinental legacy. Earth and Planetary Science Letters 157, 1-8 (1998).

14.    Evans, D. A. D. True polar wander and supercontinents. Tectonophysics 362, 303-320 (2003).

15.    Kirschvink, J. L., Ripperdan, R. L. & Evans, D. A. Evidence for a large-scale reorganization of Early Cambrian continental masses by inertial interchange true polar wander. Science 277, 541-545 (1997).

16.    Meert, J. G. A paleomagnetic analysis of Cambrian true polar wander. Earth and Planetary Science Letters 168, 131-144 (1999).

17.    Pope, M. C. & Grotzinger, J. P. Paleoproterozoic Stark Formation, Athapuscow basin, northwest Canada: Record of cratonic-scale salinity crisis. Journal of Sedimentary Research 73, 280-295 (2003).

18.    Frank, T. D. & Fielding, C. R. Marine origin for Precambrian, carbonate-hosted magnesite? Geology 31 (2003).

19.    Eugster, H. P. & Chou, I.-M. The depositional environments of Precambrian iron-formations. Economic Geology 68, 1144-1168 (1973).

20.    Álvaro, J. J. et al. Evaporitic constraints on the southward drifting of the western Gondwana margin during Early Cambrian times. Palaeogeography, Palaeoclimatology, Palaeoecology 160 (2000).

21.    Maloof, A. C., Schrag, D. P., Crowley, J. L. & Bowring, S. A. An expanded record of Early Cambrian carbon cycling from the Anti-Atlas Margin, Morocco. Canadian Journal of Earth Sciences 42, 2195-2216 (2005).

22.    Landing, E. et al. Duration of the Early Cambrian: U-Pb ages of volcanic ashes from Avalon and Gondwana. Canadian Journal of Earth Sciences 35, 329-338 (1998).

23. Powell, C. M., Li, Z. X., McElhinny, M. W., Meert, J. G. & Park, J. K. Paleomagnetic constraints on timing of the Neoproterozoic breakup of Rodinia and the Cambrian formation of Gondwana. Geology 21, 889-892 (1993).

24. Evans, D. A., Ripperdan, R. L. & Kirschvink, J. L. Polar wander and the Cambrian: response. Science 279, 9a (1998).

25. McElhinny, M. W., Powell, C. M. & Pisarevsky, S. A. Paleozoic terranes of eastern Australia and the drift history of Gondwana. Tectonophysics 362, 41-65 (2003).

26. Petrychenko, O. Y., Peryt, T. M. & Chechel, E. I. Early Cambrian seawater chemistry from fluid inclusions in halite from Siberian evaporites. Chemical Geology 219, 149-161 (2005).

27. Pisarevsky, S., Gurevich, E. & Khramov, A. N. Paleomagnetism of the Lower Cambrian sediments from the Olenek River section (northern Siberia): paleopoles and the problem of the magnetic polarity in the Early Cambrian. Geophysical Journal International 130, 746-756 (1997).

28. Smethurst, M. A., Khramov, A. N. & Torsvik, T. H. The Neoproterozoic and Palaeozoic palaeomagnetic data for the Siberian Platform: from Rodinia to Pangea. Earth-Science Reviews 43, 1-24 (1998).

29. Kirschvink, J. L. & Rozanov, A. Magnetostratigraphy of Lower Cambrian strata from the Siberian platform: a paleomagnetic pole and a preliminary polarity time-scale. Geological Magazine 121, 189-203 (1984).

30. Gallet, Y., Pavlov, V. & Courtillot, V. Magnetic reversal frequency and apparent polar wander of the Siberian platform in the earliest Palaeozoic, inferred from the Khorbusuonka river section (northeastern Siberia). Geophysical Journal International 154, 829-840 (2003).

31. Gorin, G. E., Racz, L. G. & Walter, M. R. Late Precambrian-Cambrian sediments of Huqf Group, Sultanate of Oman. American Association of Petroleum Geologists Bulletin 66, 2609-2627 (1982).

32. Mattes, B. W. & Conway Morris, S. in The Geology and Tectonics of the Oman Region (eds. Robertson, A. H. F., Searle, M. P. & Ries, A. C.) 617-636 (Geological Society, London, 1990).

33.     Amthor, J. E. et al. Extinction of Cloudina and Namacalathus at the Precambrian-Cambrian boundary in Oman. Geology 31, 431-434 (2003).

34.     Brasier, M. et al. New U-Pb zircon dates for the Neoproterozoic Ghubrah glaciation and for the top of the Huqf Supergroup, Oman. Geology 28, 175-178 (2000).

35.     Gee, E. R. in Tectonics of the Western Himalayas (eds. Malinconico, L. L., Jr. & Lillie, R. J.) 95-112 (Geological Society of America, Boulder, Colorado, 1989).

36.     Strauss, H., Banerjee, D. M. & Kumar, V. The sulfur isotopic composition of Neoproterozoic to early Cambrian seawater - evidence from the cyclic Hanseran evaporites, NW India. Chemical Geology 175, 17-28 (2001).

37.     Meert, J. G. & Van der Voo, R. Paleomagnetic and 40Ar/39Ar study of the Sinyai Dolerite, Kenya: Implications for Gondwana assembly. Journal of Geology 104, 131-142 (1996).

38.     Kirschvink, J. L. The Precambrian-Cambrian boundary problem: Paleomagnetic directions from the Amadeus basin, central Australia. Earth and Planetary Science Letters 40, 91-100 (1978).

39.     Collins, A. S. & Pisarevsky, S. A. Amalgamating eastern Gondwana: The evolution of the Circum-Indian Orogens. Earth-Science Reviews 71, 229-270 (2005).

40.     McElhinny, M. W. Palaeomagnetism of the Cambrian Purple Sandstone from the Salt Range, West Pakistan. Earth and Planetary Science Letters 8, 149-156 (1970).

41.     Preiss, W. V. in The Geology of South Australia, 1, The Precambrian (eds. Drexel, J. F., Preiss, W. V. & Parker, A. J.) 171-203 (South Australia Geological Survey, Adelaide, 1993).

42.     Rowlands, N. J., Blight, P. G., Jarvis, D. M. & von der Borch, C. C. Sabkha and playa environments in late Proterozoic grabens, Willouran Ranges, South Australia. Journal of the Geological Society of Australia 27, 55-68 (1980).

43.     Fanning, C. M., Ludwig, K. R., Forbes, B. G. & Preiss, W. V. in 8th Australian Geological Convention 71-72 (Geological Society of Australia, Adelaide, 1986).

44. Preiss, W. V. The Adelaide Geosyncline of South Australia and its significance in Neoproterozoic continental reconstruction. Precambrian Research 100, 21-63 (2000).

45. Evans, D. A. D. Stratigraphic, geochronological, and paleomagnetic constraints upon the Neoproterozoic climatic paradox. American Journal of Science 300, 347-433 (2000).

46. Fanning, C. M. & Link, P. K. U-Pb SHRIMP ages of Neoproterozoic (Sturtian) glaciogenic Pocatello Formation, southeastern Idaho. Geology 32, 881-884 (2004).

47. Wingate, M. T. D. & Giddings, J. W. Age and palaeomagnetism of the Mundine Well dyke swarm, Western Australia: implications for an Australia-Laurentia connection at 755 Ma. Precambrian Research 100, 335-357 (2000).

48. Wingate, M. T. D. & Evans, D. A. D. in Proterozoic East Gondwana: Supercontinent Assembly and Breakup (eds. Yoshida, M., Windley, B. F. & Dasgupta, S.) 77-91 (Geological Society, London, 2003).

49. Rainbird, R. H., Jefferson, C. W. & Young, G. M. The early Neoproterozoic sedimentary Succession B of northwestern Laurentia: Correlations and paleogeographic significance. Geological Society of America Bulletin 108, 454-470 (1996).

50. Harlan, S. S., Heaman, L., LeCheminant, A. N. & Premo, W. R. Gunbarrel mafic magmatic event: A key 780 Ma time marker for Rodinia plate reconstructions. Geology 31, 1053-1056 (2003).

51. Armstrong, R. L., Eisbacher, G. H. & Evans, P. D. Age and stratigraphic tectonic significance of Proterozoic diabase sheets, Mackenzie Mountains, northwestern Canada. Canadian Journal of Earth Sciences 19, 316-323 (1982).

52. Aitken, J. D. in Precambrian Sulphide Deposits (eds. Hutchinson, R. W., Spence, C. D. & Franklin, J. M.) 149-161 (Geological Association of Canada, St. Johns, Newfoundland, 1982).

53. Young, G. M., Jefferson, C. W., Delaney, G. D. & Yeo, G. M. Middle and late Proterozoic evolution of the northern Canadian Cordillera and Shield. Geology 7, 125-128 (1979).

54. Jefferson, C. W. & Ruelle, J. C. L. in Mineral Deposits of Northern Cordillera (ed. Morin, J. A.) 154-168 (Canadian Institute of Mining and Metallurgy, Montreal, 1986).

55. Palmer, H. C., Baragar, W. R. A., Fortier, M. & Foster, J. H. Paleomagnetism of Late Proterozoic rocks, Victoria Island, Northwest Territories, Canada. Canadian Journal of Earth Sciences 20, 1456-1469 (1983).

56. Park, J. K. & Jefferson, C. W. Magnetic and tectonic history of the Late Proterozoic Upper Little Dal and Coates Lake Groups of northwestern Canada. Precambrian Research 52, 1-35 (1991).

57. Behr, H. J., Ahrendt, H., Porada, H., Röhrs, J. & Weber, K. in Evolution of the Damara Orogen of South West Africa/Namibia (ed. Miller, R. M.) 1-20 (Geological Society of South Africa, Pretoria, 1983).

58. Frimmel, H. E., Klötzli, U. & Siegfried, P. New Pb-Pb single zircon age constraints on the timing of Neoproterozoic glaciation and continental break-up in Namibia. Journal of Geology 104, 459-469 (1996).

59. Frimmel, H. E., Zartman, R. E. & Späth, A. Dating Neoproterozoic continental break-up in the Richtersveld Igneous Complex, South Africa. Journal of Geology 109, 493-508 (2001).

60. Jackson, M. P. A., Warin, O. N., Woad, G. M. & Hudec, M. R. Neoproterozoic allochthonous salt tectonics during the Lufilian orogeny in the Katangan Copperbelt, central Africa. Geological Society of America Bulletin 115, 314-330 (2003).

61. Armstrong, R. A., Master, S. & Robb, L. J. Geochronology of the Nchanga Granite, and constraints on the maximum age of the Katanga Supergroup, Zambian Copperbelt. Journal of African Earth Sciences 42, 32-40 (2005).

62. Key, R. M. et al. The western arm of the Lufilian Arc in NW Zambia and its potential for copper mineralization. Journal of African Earth Sciences 33, 503-528 (2001).

63. Johnson, S. P., Rivers, T. & De Waele, B. A review of the Mesoproterozoic to early Palaeozoic magmatic and tectonothermal history of south-central Africa:

implications for Rodinia and Gondwana. Journal of the Geological Society of London 162, 433-450 (2005).

64. Grey, K. et al. Lithostratigraphic Nomenclature of the Officer Basin and Correlative Parts of the Paterson Orogen, Western Australia (Geological Survey of Western Australia, Perth, 2005).

65. Hill, A. C., Arouri, K., Gorjan, P. & Walter, M. R. in Carbonate Sedimentation and Diagenesis in the Evolving Precambrian World 327-344 (SEPM (Society for Sedimentary Geology, Tulsa, OK, 2000).

66. Hill, A. C. & Walter, M. R. Mid-Neoproterozoic (~830-750 Ma) isotope stratigraphy of Australia and global correlation. Precambrian Research 100, 181-211 (2000).

67. Walter, M. R., Veevers, J. J., Calver, C. R. & Grey, K. Neoproterozoic stratigraphy of the Centralian Superbasin, Australia. Precambrian Research 73, 173-195 (1995).

68. Pisarevsky, S. A., Li, Z. X., Grey, K. & Stevens, M. K. A palaeomagnetic study of Empress 1A, a stratigraphic drillhole in the Officer Basin: evidence for a low-latitude position of Australia in the Neoproterozoic. Precambrian Research 110, 93-108 (2001).

69. Pisarevsky, S. A., Wingate, M. T. D., Stevens, M. K. & Haines, P. W. Paleomagnetic results from the Lancer-1 stratigraphic drill hole, Officer Basin, Western Australia, and implications for Rodinia reconstructions. Australian Journal of Earth Sciences (in press).

70. Jackson, G. D. & Iannelli, T. R. in Proterozoic Basins of Canada (ed. Campbell, F. H. A.) 269-302 (Geological Survey of Canada, Ottawa, 1981).

71. Kah, L. C., Lyons, T. W. & Chesley, J. T. Geochemistry of a 1.2 Ga carbonate-evaporite succcession, northern Baffin and Bylot Islands: implications for Mesoproterozoic marine evolution. Precambrian Research 111, 203-234 (2001).

72. Fahrig, W. F., Christie, K. W. & Jones, D. L. in Proterozoic Basins of Canada (ed. Campbell, F. H. A.) 303-312 (Geological Survey of Canada, Ottawa, 1981).

73. LeCheminant, A. N. & Heaman, L. M. Mackenzie igneous events, Canada: Middle Proterozoic hotspot magmatism associated with ocean opening. Earth and Planetary Science Letters 96, 38-48 (1989).

74. Buchan, K. L. et al. Rodinia: the evidence from integrated palaeomagnetism and U-Pb geochronology. Precambrian Research 110, 9-32 (2001).

75. Benan, C. A. A. & Deynoux, M. Facies analysis and sequence stratigraphy of Neoproterozoic platform deposits in Adrar of Mauritania, Taoudeni basin, West Africa. Geologische Rundschau 87, 283-302 (1998).

76. Moussine-Pouchkine, A. & Bertrand-Sarfati, J. Tectonosedimentary subdivisions in the Neoproterozoic to Early Cambrian cover of the Taoudenni Basin (Algeria-Mauritania-Mali). Journal of African Earth Sciences 24, 425-443 (1997).

77. Clauer, N., Caby, R., Jeannette, D. & Trompette, R. Geochronology of sedimentary and metasedimentary Precambrian rocks of the West African craton. Precambrian Research 18, 53-71 (1982).

78. Teal, D. A. & Kah, L. C. Using C-isotopes to constrain intrabasinal stratigraphic correlations; Mesoproterozoic Atar Group, Mauritania. Geological Society of America, Abstracts with Programs 37, 45 (2005).

79. Perrin, M., Elston, D. P. & Moussine-Pouchkine, A. Paleomagnetism of Proterozoic and Cambrian strata, Adrar de Mauritanie, cratonic West Africa. Journal of Geophysical Research 93, 2159-2178 (1988).

80. Perrin, M. & Prévot, M. Uncertainties about the Proterozoic and Paleozoic polar wander path of the West African craton and Gondwana: evidence for successive remagnetization events. Earth and Planetary Science Letters 88, 337-347 (1988).

81. Chandler, F. W. in The Geological Environment of the Sullivan Deposit, British Columbia (eds. Lydon, J. W., Höy, T., Slack, J. F. & Knapp, M. E.) 82-112 (Geological Association of Canada, Mineral Deposits Divsion, St. Johns, Newfoundland, 2000).

82. Chandler, F. W. & Zieg, G. A. Was the depositional environment of the Sullivan Zn-Pb deposit in British Columbia marine or lacustrine and how saline was it?: a summary of the data. Geological Survey of Canada, Current Research 1994-A, 123-130 (1994).

83. White, B. Stromatolites and associated facies in shallowing-upward cycles from the middle Proterozoic Altyn Formation of Glacier National Park, Montana. Precambrian Research 24, 1-26 (1984).

84. Hietanen, A. Scapolite in the Belt Series in the St. Joe-Clearwater region, Idaho (Geological Society of America, Boulder, 1967).

85. Grotzinger, J. P. in Belt Supergroup: A Guide to Proterozoic Rocks of Western Montana and Adjacent Areas (ed. Roberts, S. M.) 143-160 (Montana Bureau of Mines and Geology, 1986).

86. Anderson, H. E. & Davis, D. W. U-Pb geochronology of the Moyie sills, Purcell Supergroup, southeastern British Columbia: implications for the Mesoproterozoic geological history of the Purcell (Belt) basin. Canadian Journal of Earth Sciences 32, 1180-1193 (1985).

87. Sears, J. W., Chamberlain, K. R. & Buckley, S. N. Structural and U-Pb geochronological evidence for 1.47 Ga rifting in the Belt basin, western Montana. Canadian Journal of Earth Sciences 35, 467-475 (1998).

88. Evans, K. V., Aleinikoff, J. N., Obradovich, J. D. & Fanning, C. M. SHRIMP U-Pb geochronology of volcanic rocks, Belt Supergroup, western Montana: evidence for rapid deposition of sedimentary strata. Canadian Journal of Earth Sciences 37, 1287-1300 (2000).

89. Elston, D. P., Enkin, R. J., Baker, J. & Kisilevsky, D. K. Tightening the Belt: Paleomagnetic-stratigraphic constraints on deposition, correlation, and deformation of the Middle Proterozoic (ca. 1.4 Ga) Belt-Purcell Supergroup, United States and Canada. Geological Society of America Bulletin 114, 619-638 (2002).

90. Muhling, P. C. & Brakel, A. T. Geology of the Bangemall Group - The evolution of an intracratonic Proterozoic basin (Geological Survey of Western Australia, Perth, 1985).

91. Martin, D. M. & Thorne, A. M. Tectonic setting and basin evolution of the Bangemall Supergroup in the northwestern Capricorn Orogen. Precambrian Research 128, 385-409 (2004).

92.   Jackson, M. J., Muir, M. D. & Plumb, K. A. Geology of the southern McArthur Basin, Northern Territory (Bureau of Mineral Resources, Canberra, 1987).

93.   Sami, T. T. et al. in Carbonate Sedimentation and Diagenesis in the Evolving Precambrian World (eds. Grotzinger, J. P. & James, N. L.) 243-274 (SEPM (Society of Sedimentary Geology), Tulsa, OK, 2000).

94.   Walker, R. N., Muir, M. D., Diver, W. L., Williams, N. & Wilkins, N. Evidence of major sulphate evaporite deposits in the Proterozoic McArthur Group, Northern Territory, Australia. Nature 265, 526-529 (1977).

95.   Idnurm, M. Towards a high resolution Late Palaeoproterozoic - earliest Mesoproterozoic apparent polar wander path for northern Australia. Australian Journal of Earth Sciences 47, 405-429 (2000).

96.   Southgate, P. N. et al. Basin shape and sediment architecture in the Gun Supersequence: a strike-slip model for Pb-Zn-Ag ore genesis at Mt Isa. Australian Journal of Earth Sciences 47, 509-531 (2000).

97.   Page, R. W., Jackson, M. J. & Krassay, A. A. Constraining sequence stratigraphy in north Australian basins: SHRIMP U-Pb zircon geochronology between Mt Isa and McArthur River. Australian Journal of Earth Sciences 47, 431-459 (2000).

98.   Idnurm, M., Giddings, J. W. & Plumb, K. A. Apparent polar wander and reversal stratigraphy of the Palaeo-Mesoproterozoic southeastern McArthur Basin, Australia. Precambrian Research 72, 1-41 (1995).

99.   Betts, P. G. et al. Synthesis of the Proterozoic evolution of the Mt Isa Inlier. Australian Journal of Earth Sciences 53, 187-211 (2006).

100.  Southgate, P. N. et al. Chronostratigraphic basin framework for Palaeoproterozoic rocks (1730-1575 Ma) in northern Australia and implications for base-metal mineralisation. Australian Journal of Earth Sciences 47, 461-483 (2000).

101.  Lindsay, J. F. & Brasier, M. D. A carbon isotope reference curve for ca. 1700-1575 Ma, McArthur and Mount Isa Basins, Northern Australia. Precambrian Research 99, 271-308 (2000).

102.  Bradshaw, B. E., Lindsay, J. F., Krassay, A. A. & Wells, A. T. Attenuated basin-margin sequence stratigraphy of the Palaeoproterozoic Calvert and Isa

Superbasins: the Fickling Group, southern Murphy Inlier, Queensland. Australian Journal of Earth Sciences 47, 599-623 (2000).

103.    Krassay, A. A., Bradshaw, B. E., Domagala, J. & Jackson, M. J. Siliciclastic shoreline to growth-faulted, turbiditic sub-basins: the Proterozoic River Supersequence of the upper McNamara Group on the Lawn Hill Platform, northern Australia. Australian Journal of Earth Sciences 47, 533-562 (2000).

104.    Domagala, J., Southgate, P. N., McConachie, B. A. & Pidgeon, B. A. Evolution of the Palaeoproterozoic Prize, Gun and lower Loretta Supersequences of the Surprise Creek Formation and Mt Isa Group. Australian Journal of Earth Sciences 47, 485-507 (2000).

105.    Jackson, M. J. & Southgate, P. N. Evolution of three unconformity-bounded sandy carbonate successions in the McArthur River region of northern Australia: the Lawn, Wide and Doom Supersequences in a proximal part of the Isa Superbasin. Australian Journal of Earth Sciences 47, 625-635 (2000).

106.    Badham, J. P. N. & Stanworth, C. W. Evaporites from the lower Proterozoic of the East Arm, Great Slave Lake. Nature 268, 516-518 (1977).

107.    Hoffman, P. F., Bell, I. R., Hildebrand, R. S. & Thorstad, L. Geology of the Athapuscow Aulacogen, east arm of Great Slave Lake, District of Mackenzie. Geological Survey of Canada, Report of Activities, Part A 77-1A, 117-129 (1977).

108.    Stanworth, C. W. & Badham, J. P. N. Lower Proterozoic red beds, evaporites and secondary sedimentary uranium deposits from the East Arm, Great Slave Lake, Canada. Journal of the Geological Society of London 141, 235-242 (1984).

109.    Bowring, S. A., Van Schmus, W. R. & Hoffman, P. F. U-Pb zircon ages from Athapuscow Aulacogen, East Arm of Great Slave Lake, N.W.T., Canada. Canadian Journal of Earth Sciences 21, 1315-1324 (1984).

110.    Hoffman, P. F. & Grotzinger, J. P. Orographic precipitation, erosional unloading, and tectonic style. Geology 21, 195-198 (1993).

111.    Bingham, D. K. & Evans, M. E. Paleomagnetism of the Great Slave Supergroup, Northwest Territories, Canada: the Stark Formation. Canadian Journal of Earth Sciences 13, 563-578 (1976).

112. Irving, E., Baker, J., Hamilton, M. & Wynne, P. J. Early Proterozoic geomagnetic field in western Laurentia: implications for paleolatitudes, local rotations, and stratigraphy. Precambrian Research 129, 251-270 (2004).

113. Evans, M. E. & Bingham, D. K. Paleomagnetism of the Great Slave Supergroup, Northwest Territories, Canada: the Tochatwi Formation. Canadian Journal of Earth Sciences 13, 555-562 (1976).

114. Grotzinger, J. P. Cyclicity and paleoenvironmental dynamics, Rocknest platform, northwest Canada. Geological Society of America Bulletin 97, 1208-1231 (1986).

115. Bowring, S. A. & Grotzinger, J. P. Implications of new chronostratigraphy for tectonic evolution of Wopmay Orogen, northwest Canadian Shield. American Journal of Science 292, 1-20 (1992).

116. Evans, M. E. & Hoye, G. S. in Proterozoic Basins of Canada (ed. Campbell, F. H. A.) 191-202 (Geological Survey of Canada, Ottawa, 1981).

117. El Tabakh, M., Grey, K., Pirajno, F. & Schreiber, B. C. Pseudomorphs after evaporitic minerals interbedded with 2.2 Ga stromatolites of the Yerrida basin, Western Australia: Origin and significance. Geology 27, 871-874 (1999).

118. Melezhik, V. A., Fallick, A. E., Medvedev, P. V. & Makarikhin, V. V. Extreme $^{13}C_{carb}$ enrichment in ca. 2.0 Ga magnesite-stromatolite-dolomite-'red beds' association in a global context: a case for the world-wide signal enhanced by a local environment. Earth-Science Reviews 48, 71-120 (1999).

119. Melezhik, V. A., Fallick, A. E., Rychanchik, D. V. & Kuznetsov, A. B. Palaeoproterozoic evaporites in Fennoscandia: implications for seawater sulphate, the rise of atmospheric oxygen and local amplification of the $d^{13}C$ excursion. Terra Nova 17, 141-148 (2005).

120. Schidlowski, M., Eichmann, R. & Junge, C. E. Precambrian sedimentary carbonates: Carbon and oxygen isotope geochemistry and implications for the terrestrial oxygen budget. Precambrian Research 2, 1-69 (1975).

121. Karhu, J. A. & Holland, H. D. Carbon isotopes and the rise of atmospheric oxygen. Geology 24, 867-870 (1996).

122. Torsvik, T. H. & Meert, J. G. Early Proterozoic palaeomagnetic data from the Pechenga Zone (north-west Russia) and their bearing on Early Proterozoic palaeogeography. Geophysical Journal International 122, 520-536 (1995).

123. Larue, D. K. The Chocolay Group, Lake Superior region, U.S.A.: Sedimentologic evidence for deposition in basinal and platform settings on an early Proterozoic craton. Geological Society of America Bulletin 92, 417-435 (1981).

124. Young, G. M. Stratigraphic and tectonic settings of Proterozoic glaciogenic rocks and banded iron-formations: relevance to the snowball Earth debate. Journal of African Earth Sciences 35, 451-466 (2002).

125. Cameron, E. M. Evidence from early Proterozoic anhydrite for sulphur isotopic partitioning in Precambrian oceans. Nature 304, 54-56 (1983).

126. Chandler, F. W. in Sediment-hosted stratiform copper deposits (eds. Boyle, R. W., Brown, A. C., Jefferson, C. W., Jowett, E. C. & Kirkham, R. V.) 225-244 (Geological Association of Canada, Toronto, 1989).

127. Corfu, F. & Andrews, A. J. A U-Pb age for mineralized Nipissing diabase, Gowganda, Ontario. Canadian Journal of Earth Sciences 23, 107-109 (1986).

128. Noble, S. R. & Lightfoot, P. C. U-Pb baddeleyite ages of the Kerns and Triangle Mountain intrusions, Nipissing Diabase, Ontario. Canadian Journal of Earth Sciences 29, 1424-1429 (1992).

129. Krogh, T. E., Davis, D. W. & Corfu, F. in The Geology and Ore Deposits of the Sudbury Structure (eds. Pye, E. G., Naldrett, A. J. & Giblin, P. E.) 431-446 (Ontario Geological Survey, 1984).

130. Chown, E. H. Tourmalinites in the Aphebian Mistassini Group, Quebec. Canadian Journal of Earth Sciences 24, 826-830 (1987).

131. Williams, G. E. & Schmidt, P. W. Paleomagnetism of the Paleoproterozoic Gowganda and Lorrain formations, Ontario: low paleolatitude for Huronian glaciation. Earth and Planetary Science Letters 153, 157-169 (1997).

132. Hilburn, I. A. et al. A negative fold test on the Lorrain Formation of the Huronian Supergroup: Uncertainty on the paleolatitude of the Paleoproterozoic Gowganda glaciation and implications for the great oxygenation event. Earth and Planetary Science Letters 232, 315-332 (2005).